

# CGC/saturation approach: re-visiting the problem of odd harmonics in angular correlations

E. Gotsman<sup>1,a</sup>, E. Levin<sup>1,2,b</sup>

<sup>1</sup> Department of Particle Physics, School of Physics and Astronomy, Raymond and Beverly Sackler Faculty of Exact Science, Tel Aviv University, 69978 Tel Aviv, Israel

<sup>2</sup> Departamento de Física, Centro Científico- Tecnológico de Valparaíso, Universidad Técnica Federico Santa María, Avda. Espana 1680, Casilla 110-V, Valparaíso, Chile

Received: 23 July 2018 / Accepted: 15 September 2018 / Published online: 28 September 2018  
© The Author(s) 2018

**Abstract** In this paper we demonstrate that the selection of events with different multiplicities of produced particles, leads to the violation of the azimuthal angular symmetry,  $\phi \rightarrow \pi - \phi$ . We find for LHC and lower energies, that this violation can be so large for the events with multiplicities  $n \geq 2\bar{n}$ , where  $\bar{n}$  is the mean multiplicity, that it leads to almost no suppression of  $v_n$ , with odd  $n$ . However, this can only occur if the typical size of the dipole in DIS with a nuclear target is small, or  $Q^2 > Q_s^2(A; Y_{\min}, b)$ , where  $Q_s$  is the saturation momentum of the nucleus at  $Y = Y_{\min}$ . In the case of large sizes of dipoles, when  $Q^2 < Q_s^2(A; Y_{\min}, b)$ , we show that  $v_n = 0$  for odd  $n$ . Hadron-nucleus scattering is discussed.

## Contents

1 Introduction	1
2 The dilute–dilute system scattering: $\phi \rightarrow \pi - \phi$ symmetry and its violation	2
3 The BFKL Pomeron calculus in zero transverse dimensions: correlations in hadron–nucleus scattering	5
3.1 Generalities	5
3.2 Healing the Finkelstein–Kajantie disease	6
3.3 Generating functional for the production processes	7
3.4 Schwimmer model for hadron–nucleus scattering with induced $\phi \rightarrow \pi - \phi$ symmetry: $v_{n,n}$ and $v_n$	9
4 QCD cascade	11
4.1 The simplified non-linear equation	11
4.2 Solution	12

4.2.1 Perturbative QCD region ( $\tau < 1$ )	12
4.2.2 Saturation region ( $\tau > 1$ )	12
4.3 Formulation of the problem	12
4.4 Processes with different multiplicities of produced gluons for $\tau_m \ll 1$	13
4.5 Estimates for proton–nucleus scattering	14
4.6 Processes with different multiplicities of produced gluons for $\tau_m \geq 1$	15
5 Conclusions	17
References	17

## 1 Introduction

In this paper we continue to discuss the azimuthal long range rapidity correlations. These correlations were measured in all reactions: hadron–hadron, hadron–nucleus and nucleus–nucleus scattering, and they have similar features independent of the reactions [1–17]. Such similarity in energy, multiplicity and transverse momentum dependence as well as in the values of the harmonics  $v_n$ , calls for a general explanation. We believe that the source of these correlations is the Bose–Einstein enhancement for identical gluons. The origin does not depend on the type of the reaction, and we have demonstrated that this mechanism alone is able to describe all the experimental data [18–20]. However, in the effective theory of high energy QCD: CGC/saturation approach (see Ref. [21] for a review) the resulting angular correlation leads to  $v_n = 0$  for all odd  $n$  [22–27] (see also Refs. [28,29]). This stems from the symmetry  $\phi \rightarrow \pi - \phi$ , where  $\phi$  is the azimuthal angle which is implicitly contained in the CGC/saturation approach. This symmetry does not result from any fundamental principle, and only arises in the leading order of the approach. Several efforts to calculate corrections to the leading order CGC/saturation approach have been made (see Refs. [19,27,30] which demonstrated that

<sup>a</sup> e-mail: gotsman@post.tau.ac.il

<sup>b</sup> e-mails: leving@post.tau.ac.il; eugeniy.levin@usm.cl

this correction violates the symmetry which lead to a  $v_n$  for odd  $n$ . If these corrections originate from the next-to-leading order corrections, they should have a parametrically strong suppression, while experimentally  $v_3 < v_2$  but  $v_3 \approx v_4$ . If we believe that the CGC/saturation approach in leading order describes all other physical observables, then we interpret the experimental results, as an indication that the suppression of  $v_3$  is of a numerical nature.

The main idea of this paper is that selection by the multiplicity of the event, destroys this symmetry, and leads to  $v_n \neq 0$  for odd  $n$ . We consider the deep inelastic scattering on nuclei, which has the most solid theoretical description in the framework of the CGC/saturation approach, and allows one to investigate the dependence of the effect on the size of the interacting dipoles.

The main result of this paper is that, by selecting the event with given multiplicity, leads to a strong violation of the symmetry in the leading order of the CGC/saturation estimates. We show that the violation of this symmetry depends crucially on the sizes of the interacting dipoles. For DIS with virtuality of photon  $Q$ , we have two distinct regions. For  $Q_s^2(A, Y_{\min}; b)/Q^2 \leq 1$  (where  $Q_s$  denotes the saturation scale and  $Y_{\min}$  is the minimal value of the rapidity at which we can use CGC approach), it turns out that the violation of the symmetry is so strong for the events with multiplicities,  $n \geq 2\bar{n}$ <sup>1</sup> that there is practically no suppression of the values of  $v_n$  at odd  $n$ . However, on the other hand for  $Q_s^2(A, Y_{\min}; b)/Q^2 \geq 2$ , we have to deal with the violation of the geometric scaling behaviour of the scattering amplitude in the saturation domain, this results in the restoration of the  $\phi \rightarrow \pi - \phi$  symmetry, for the events with multiplicities  $n \geq 2\bar{n}$ .

In the next section we discuss the origin of the azimuthal angular symmetry,  $\phi \rightarrow \pi - \phi$ , for the dilute–dilute parton systems scattering in the entire inclusive measurements, and show that this symmetry stems from the mixture of events with low multiplicity: multiplicity which is less than the average multiplicity  $\bar{n}$ , and events with high multiplicity, more or equal to  $2\bar{n}$ . In Sect. 3 we discuss angular correlations in a  $1 + 1$  dimensional toy model, which can be considered as a theory which describes the interaction between QCD partons of the fixed sizes. We demonstrate, that in this model,  $\phi \rightarrow \pi - \phi$  symmetry is reproduced for the entire inclusive measurement. However, the selection of events with fixed multiplicity violates this symmetry. Our estimates shows, this violation is so strong, that for the measurement of the events with multiplicities  $n \geq 2\bar{n}$ ,  $\bar{n}$  denotes the mean multiplicity in the process, does not lead to the suppression of  $v_n$  for odd  $n$ . In Sect. 4 we consider the CGC/saturation approach with a

simplified model for the BFKL kernel. For this approach we develop a procedure to calculate the double inclusive cross section for two gluon production for the events with different multiplicities.

For LHC or lower energies, in the kinematic region where  $Q_s^2(A, Y_{\min}; b)/Q^2 \leq 1$  and for events with multiplicities  $n \geq 2\bar{n}$ , our estimates result in a small enhancing factor for  $v_n$  with even  $n$ , and a damping factor for  $v_n$  with odd  $n$ . However, we show that for  $Q_s^2(A, Y_{\min}; b)/Q^2 \geq 2$  we face a problem of the violation of the geometric scaling behaviour of the scattering amplitude in the saturation domain, which leads to the restoration of the  $\phi \rightarrow \pi - \phi$  symmetry in the events with  $n \geq 2\bar{n}$ . In the Conclusions we summarize our results.

## 2 The dilute–dilute system scattering: $\phi \rightarrow \pi - \phi$ symmetry and its violation

The long range rapidity correlation for the dilute–dilute system scattering (DIS on a proton target) stems from the two parton shower production, and can be described by the Mueller diagrams shown in Fig. 1. These diagrams give the following expression for the double inclusive cross section for the diagram of Fig. 1a:

$$\begin{aligned} & \frac{d\sigma(\text{Fig. 1a})}{dy_1 d^2p_{1T} dy_2 d^2p_{2T}} \\ & \propto \int d^2Q_T N_{\gamma^*}(Q, Q_T) N(Q_T) \\ & \times \frac{\bar{\alpha}_S}{p_{1T}^2} \int d^2k_T \phi^{\text{BFKL}}(Y - y_1, k_T, Q_T) \\ & \times \frac{\Gamma_\mu(k_T, p_{1T}) \Gamma_\mu(k_T, p_{1T})}{k_T^2 (\mathbf{k}_T - \mathbf{p}_{1T})^2} \phi^{\text{BFKL}}(y_1, k_T, Q_T) \\ & \times \frac{\bar{\alpha}_S}{p_{2T}^2} \int d^2l_T \phi^{\text{BFKL}}(Y - y_2, l_T, -Q_T) \\ & \times \frac{\Gamma_\mu(l_T, p_{2T}) \Gamma_\mu(l_T, p_{2T})}{l_T^2 (\mathbf{l}_T - \mathbf{p}_{2,T})^2} \phi^{\text{BFKL}}(y_1, l_T, -Q_T) \quad (1) \end{aligned}$$

In Eq. (1)  $\phi$  at  $Q_T = 0$  is the solution of the BFKL equation

$$\begin{aligned} \frac{\partial \phi^{\text{BFKL}}(y, \mathbf{k}_T)}{\partial y} &= \bar{\alpha}_S \int \frac{d^2k'_T}{\pi} \frac{1}{(\mathbf{k}_T - \mathbf{k}'_T)^2} \phi^{\text{BFKL}}(y, \mathbf{k}'_T) \\ & - 2\omega_G(\mathbf{k}_T) \phi^{\text{BFKL}}(y, \mathbf{k}_T); \quad (2) \end{aligned}$$

where

$$\begin{aligned} \omega_G(\mathbf{k}_T) &= \frac{1}{2} \bar{\alpha}_S k_T^2 \int \frac{d^2k'_T}{2\pi} \frac{1}{k_T'^2 (\mathbf{k}_T - \mathbf{k}'_T)^2} \\ &= \bar{\alpha}_S k_T^2 \int \frac{d^2k'_T}{2\pi} \frac{1}{(k_T'^2 + (\mathbf{k}_T - \mathbf{k}'_T)^2) (\mathbf{k}_T - \mathbf{k}'_T)^2} \quad (3) \end{aligned}$$

<sup>1</sup>  $Q_s(A, Y_{\min}; b)$  is the saturation moment of the nucleus at low energies (minimal rapidity  $Y_{\min}$ ) at fixed impact parameter  $b$ .  $\bar{n}$  denotes the mean multiplicity in the reaction at fixed rapidity  $Y$ .

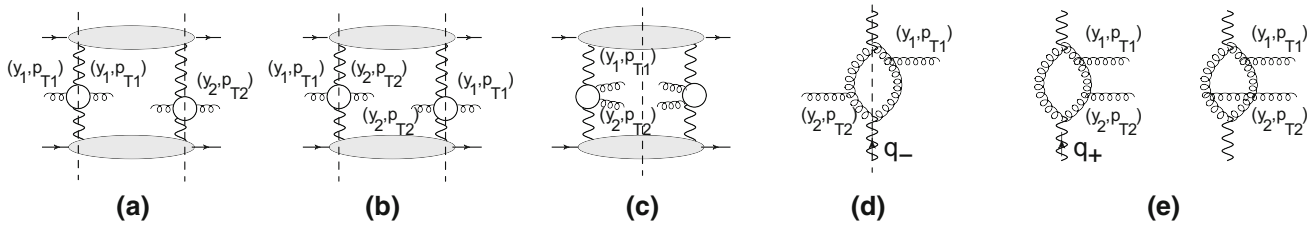


**Fig. 1** Mueller diagrams [31] for the angular correlations for dilute-dilute system scattering (DIS on a proton target). **a** Double inclusive production from two parton showers (two cut BFKL Pomeron [32–34]). **b** (interference diagram): the Bose–Einstein correlations of two identical gluons from two parton showers (two cut BFKL Pomeron). **c** Central diffractive production of two gluons in the colorless state. **d** The structure of the vertex for emission of two identical gluons in the interference diagram. **e** The vertex for emission of two gluons in the colorless state in central diffractive production. Wavy lines denote

the BFKL Pomeron. The vertical dotted lines indicate the final state that is measured by the detectors. The wavy lines with a vertical dotted line, denote the cut Pomeron which corresponds to the gluons produced in a one parton shower. Its structure is shown in Fig. 3. Helical lines describe gluons. The blobs correspond to the amplitude for Pomeron–hadron ( $\gamma^*$ ) scattering, which is integrated over the energy ( $N(Q_T)$ ,  $N_{\gamma^*}(Q, Q_T)$ ). This integral depends only on the transverse momentum of the Pomeron ( $Q_T$ )

For  $Q_T \neq 0$  the expressions for  $\phi$  appear a bit more complicated, however, we do not need to know them, as the  $Q_T$  dependence of the BFKL equation is determined by the size of the largest interacting dipoles. In Fig. 1 these sizes are of the order of the sizes of hadrons, which are much larger than  $1/p_{iT}$ . Therefore, we can neglect  $Q_T$  in comparison with  $p_{iT}$  and  $k_T$  or  $l_T$ , which are of the order of  $p_{iT}$ .

The diagram of Fig. 1a generates the rapidity correlations, but not correlations in the azimuthal angle. The latter stem from two different sources: the Bose–Einstein correlations of the identical gluons, given by the diagram of Fig. 1b; and the central diffractive production of two gluons in a colourless state (see Fig. 1c). Both, have similar expressions. For Fig. 1b we have

$$\begin{aligned} & \frac{d\sigma(\text{Fig. 1b})}{dy_1 d^2 p_{1T} dy_2 d^2 p_{2T}} \\ & \propto \frac{1}{N_c^2 - 1} \int d^2 Q_T N_{\gamma^*}(Q, Q_T) N(Q_T + q_-) \\ & \times \frac{\bar{\alpha}_S}{p_{1T}^2} \int d^2 k_T \phi^{\text{BFKL}}(Y - y_1, k_T, Q_T) \\ & \times \frac{\Gamma_\mu(k_T, p_{1T}) \Gamma_\mu(k_T, p_{2T})}{k_T^2 (\mathbf{k}_T - \mathbf{p}_{1T})^2} \phi^{\text{BFKL}}(y_2, k_T, Q_T) \\ & \times \frac{\bar{\alpha}_S}{p_{2T}^2} \int d^2 l_T \phi^{\text{BFKL}}(Y - y_1, l_T, -Q_T) \\ & \times \frac{\Gamma_\mu(l_T, p_{1T}) \Gamma_\mu(l_T, p_{2T})}{l_T^2 (\mathbf{l}_T - \mathbf{p}_{2T})^2} \phi^{\text{BFKL}}(y_2, l_T, -Q_T) \end{aligned} \quad (4)$$

with  $q_- = \mathbf{p}_{1T} - \mathbf{p}_{2T}$ . For small  $y_{12} = y_1 - y_2$  ( $\bar{\alpha}_S y_{12} \ll 1$ ) the arguments of  $\phi$ 's in both equations are the same, and the correlation function has the form:

$$\begin{aligned} & C^{\text{BE}}(L_c | q_{-,T} |) \\ & = \frac{1}{N_c^2 - 1} \frac{\int d^2 Q_T N_{\gamma^*}(Q, Q_T) N(Q_T + q_{-,T})}{\int d^2 Q_T N(Q_T) N(Q_T)} \end{aligned} \quad (5)$$

From Eq. (5) one can see that the correlation length  $L_c$  is determined by the dimensional scales of the amplitude  $N$ . We have two distinct scales in this amplitude, which can be seen from the following expression (see Fig. 2 and Ref. [26]):

$$\begin{aligned} & N_{\gamma^*}(Q, Q_T) \\ & = \int d^2 k_T d^2 l_T I_P(\mathbf{k}_T, \mathbf{l}_T, -\mathbf{l}_T + \mathbf{Q}_T, -\mathbf{k}_T + \mathbf{Q}_T) \\ & + \int_{y_M \gg 1} d y_M \phi^{\text{BFKL}}(y_M, Q, Q_T = 0) G_{3P}(Q_s(y_M), Q_T) \\ & N(Q_T) = \int d M^2 \left( \sum_{i=1}^{M_0} G_i^2(Q_T) \delta(M^2 - M_i^2) \right. \\ & \left. + \phi^{\text{BFKL}}(y_M \geq y_{M_0}, k_T, Q_T = 0) G_{3P}(Q_s(y_M), Q_T) \right) \end{aligned} \quad (6)$$

where

$$\begin{aligned} & F(Q_T) = \int d^2 r dz e^{i \frac{1}{2} Q_T \cdot r} |\Psi_{\gamma^*}(Q, z, r)|^2 \\ & I_P(\mathbf{k}_T, \mathbf{l}_T, -\mathbf{l}_T + \mathbf{Q}_T, -\mathbf{k}_T + \mathbf{Q}_T) \\ & = 1 + F(2Q_T) + F(2(\mathbf{k}_T + \mathbf{l}_T)) \\ & \quad + F(2(\mathbf{k}_T - \mathbf{l}_T - Q_T)) \\ & \quad - F(2k_T) - F(2(\mathbf{k}_T - Q_T)) \\ & \quad - F(2l_T) - F(2(\mathbf{l}_T + Q_T)) \end{aligned} \quad (7)$$

and  $\phi^{\text{BFKL}}(y_M, Q, Q_T = 0)$  denotes the unintegrated gluon structure function that describes the BFKL evolution from the transverse momentum  $Q_s(y_M)$  to  $Q^2$ . The dependence of  $G_{3P}$  on  $Q_T$  has been discussed in Ref. [26]. The sum over resonance contributions leads to a scale of about the size of the hadron, while the triple Pomeron contribution for a rapidity  $y_M = \ln(M^2/M_0^2)$ , generates a scale which is of the order of the saturation scale.

**Fig. 2** The graphic form of Eq. (6) :  $N(Q_T)$  for proton (a) and  $N_{\gamma^*}$  for DIS (b) Large blue blob shows the triple Pomeron vertex. The wavy lines describe the BFKL Pomerons

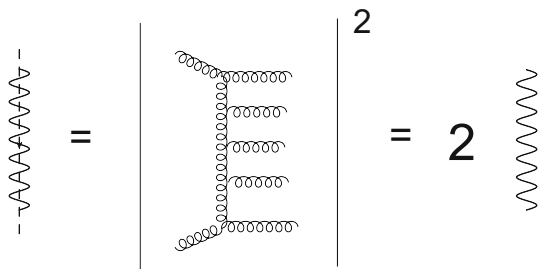
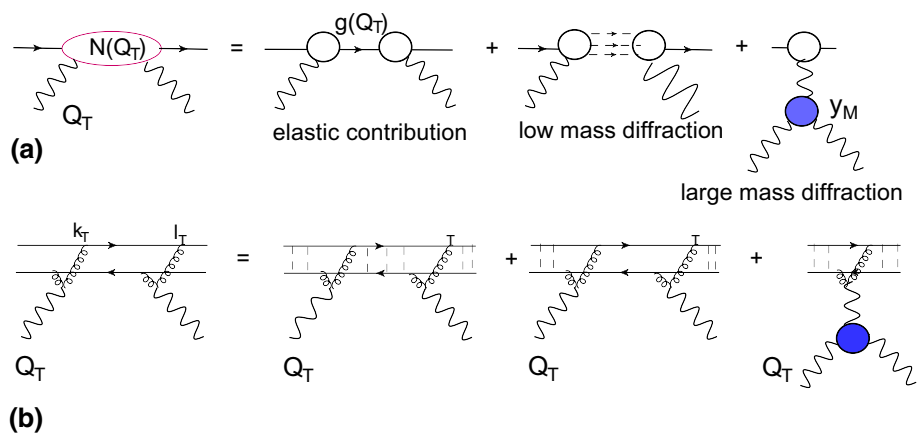


**Fig. 3** The graphic form of the unitarity constraint (see Eq. (8))

Equation (5) does not have a symmetry for  $\phi \rightarrow \pi - \phi$ , and generates harmonics  $v_n$  both with even and odd  $n$ . The Mueller diagram of Fig. 1b describes the interference between two produced parton showers, since the cut Pomeron is related to the production of the single parton shower, as shown in Fig. 3. From the unitarity constraint

$$2 \text{Im}A_{el}(s, b; r) = \underbrace{|A_{el}(s, b; r)|^2}_{\text{elastic cross section}} + \underbrace{G(s, b, r)}_{\text{inelastic processes}} \rightarrow 2 \text{Im}G_{\mathbb{P}}^{\text{BFKL}}(s, b; r) = G(s, b, r) = \text{cut Pomeron} \tag{8}$$

since the contributions of  $|A_{el}(s, b; r)|^2$ , in the leading  $\log(1/x)$  approximation of perturbative QCD (LL(1/x)A), it turns out to be negligibly small.

Equation (5) describes the correlations that stem from the event with large multiplicity of the order of  $2\bar{n}$ , where  $\bar{n}$  denotes the multiplicity of the one parton shower. We need to add the emission of two gluons in the colorless state, produced in the central diffraction process shown in Fig. 1c. Generally speaking, the BFKL Pomerons in this diagram are different from those in Fig. 1b, since the momenta transferred by these Pomerons have longitudinal components  $Q_L$  and  $Q_L - q_{+,L}$ . However, in the leading order they can be neglected. The vertex for the production of two gluons (see Fig. 1e), turns out to be twice larger (see Appendix B in Ref. [19]) than the vertex of the gluon emission (see

Fig. 1d). This results in the same contribution of this diagram, as of the diagrams of Fig. 1b with the only difference: the BFKL Pomeron carry momenta  $Q_T$  and  $Q_T + q_{+,T}$  where  $q_{+,T} = p_{1T} + p_{2T}$ . Hence this diagram generates the correlation function which is equal to

$$C^{\text{CD}}(L_c|q_{+,T}|) = \frac{1}{N_c^2 - 1} \frac{\int d^2 Q_T N_\gamma(Q, Q_T) N(Q_T + q_{+,T})}{\int d^2 Q_T N(Q_T) N(Q_T)} \tag{9}$$

The sum  $C^{\text{CD}}(L_c|q_{+,T}|) + C^{\text{BE}}(L_c|q_{-,T}|)$  has the symmetry  $\phi \rightarrow \pi - \phi$ . It should be emphasized that this symmetry is a direct consequence of an entirely inclusive measurement, without any selection of the event accordingly to multiplicity.

However, one can see that this symmetry stems from the mixture of two events with quite different multiplicities: diagrams of Fig. 1a and b describe the events with the multiplicity  $n = 2\bar{n}$ , while the diagram of Fig. 1-c correspond to the events with low multiplicities  $n \ll \bar{n}$ . In other words, if we select events with large multiplicities so that  $n \geq 2\bar{n}$ , we have no  $\phi \rightarrow \pi - \phi$  symmetry, and the source for the azimuthal angular correlation is the Bose–Einstein enhancement.

It is instructive to note, that for the entire inclusive measurement, this symmetry is not violated in the next to leading approximation. For a dilute–dilute system the first corrections are related to accounting for the one Pomeron loop (see Fig. 4). In inclusive measurements, we take into account the processes of two gluon diffractive production given by Fig. 4a1 and b1. Figure 4a1 describes the process of central diffractive production with low multiplicity, while Fig. 4b1 shows the diffractive production which is accompanied by the multi-gluon generation from the one parton shower, with multiplicity  $\bar{n}$ . In Fig. 4c1 and d1 the double inclusive cross sections are shown for the event with multiplicities  $2\bar{n}$  (Fig. 4c1) and  $3\bar{n}$  (Fig. 4d1). Figure 4a–d demonstrate the AGK cutting rules and provide the weight of the processes with different multiplicities:  $n \ll \bar{n}, \bar{n}, 2\bar{n}$  and  $3\bar{n}$ , respectively. Taking into account the simple combinatorics for two

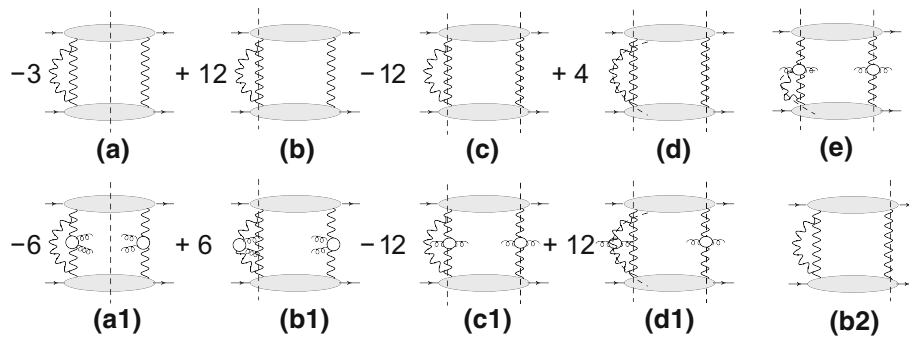


**Fig. 4** AGK [45,46] cutting rules for the exchange of three Pomerons (a–d) and Mueller diagrams for the central diffractive production of two gluons (a1, b1) and for two particle correlations (c1, d1). e is the diagram that can violate the AGK cutting rules. However, this diagram

accounts for the Pomeron loop of the size of  $Y/2$ , where  $Y$  is the total rapidity. Hence, the contribution of this diagram turns out to be much smaller than the contributions of the diagrams a1 and b1. The notations are the same as in Fig. 1

gluon diffractive emission, and the emissions from the different parton showers shown in Fig. 4a1–d1, one can see, that the double gluon cross sections and the central diffractive contributions, are the same as for the emission of the two gluon showers. In other words, in the next-to-leading order diagrams, the contributions with different multiplicities are canceled, leading to vanishing contributions for inclusive measurements. We postpone the calculation of the combinatoric coefficient to the next section, but we would like to note that central diffraction can come from the diagram of Fig. 4b1, but it cannot originate from the diagram of Fig. 4b2. Hence, the symmetry  $\phi \rightarrow \pi - \phi$  is not violated in the next-to-leading order. It shows that the symmetry  $\phi \rightarrow \pi - \phi$  is an inherent feature of QCD, at least in the leading  $\log(1/x)$  approximation.

The contribution of the first Pomeron loop is well known, and its calculation leads to lengthy and cumbersome formulae, which can be found in Refs. [35–44]. Our strategy is to clarify all essential points using the simplified version of the Pomeron calculus in  $1 + 1$  space-time, which we discuss in the next section.

Prior to doing so, we wish to comment on the AGK cutting rules in QCD. The AGK cutting rules have been discussed and proven in Refs. [47–53] for the inclusive cross sections. In Ref. [54] it is shown that the AGK cutting rules are violated for double inclusive production. This violation is intimately related to the enhanced diagrams [53,54], and reflects the fact that different cuts of the triple BFKL Pomeron vertex, lead to different contributions, as can be seen from Figs. 1 and 4. We will not consider such diagrams. In principle, we can consider diagrams of the type of Fig. 4e, however, these diagrams correspond to the contribution of the small Pomeron loop ( $\sim Y/2$ , where  $Y$  is the total rapidity). Hence, their contributions are small compared to the diagrams Fig. 4a1 and b1.

### 3 The BFKL Pomeron calculus in zero transverse dimensions: correlations in hadron–nucleus scattering

#### 3.1 Generalities

In this section we consider a simplified model for the Pomeron interaction, in which we neglect the fact that this interaction can change the sizes of dipoles [58–61] (Fig. 5). In such an approach the DIS process with a nucleus target appears to be the same as proton–nucleus scattering. In this model the scattering amplitude ( $N$ ) is a function of one variable:  $Y$  for which we have a simplified Balitsky–Kovchegov equation [55–57] of the form:

$$\frac{dN(Y)}{dY} = \Delta \left( N(Y) - N^2(Y) \right) \tag{10}$$

The solution to this equation has the form

$$N(Y) = \frac{\gamma e^{\Delta Y}}{1 + \gamma (e^{\Delta Y} - 1)} = \frac{\gamma z}{1 + \gamma (z - 1)} \tag{11}$$

where  $N(Y = 0) = \gamma$  and  $z = e^{\Delta Y}$ . In the linear approximation, when  $N^2 \ll N$  Eq. (11) degenerates to

$$\frac{dN(Y)}{dY} = \Delta N(Y) \tag{12}$$

hence,  $\Delta$  is the intercept of the BFKL Pomeron.

The equation for the process of the diffractive dissociation which was proven in QCD [62], transforms into the following equation in the framework of the BFKL Pomeron calculus in zero transverse dimension [62–64]:

$$\begin{aligned} \frac{dN^D(Y, Y_{min})}{d\Delta Y} &= N^D(Y, Y_{min}) + \left( N^D(Y, Y_{min}) \right)^2 \\ &- 2(N(Y) + \bar{N}(Y)) N^D(Y, Y_{min}) \\ &+ 2N(Y) \bar{N}(Y) \end{aligned} \tag{13}$$

**Fig. 5** The graphic form of the equation of Ref. [62] for diffractive production ( $N^D$ ) in the BFKL Pomeron calculus, in zero transverse dimensions.  $N$  and  $\bar{N}$  denote the elastic amplitudes with initial conditions:  $N(Y=0) = \gamma$  and  $\bar{N}(Y=0) = \bar{\gamma}$

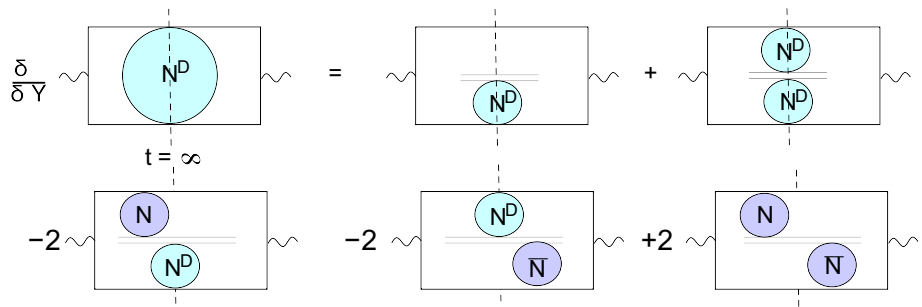
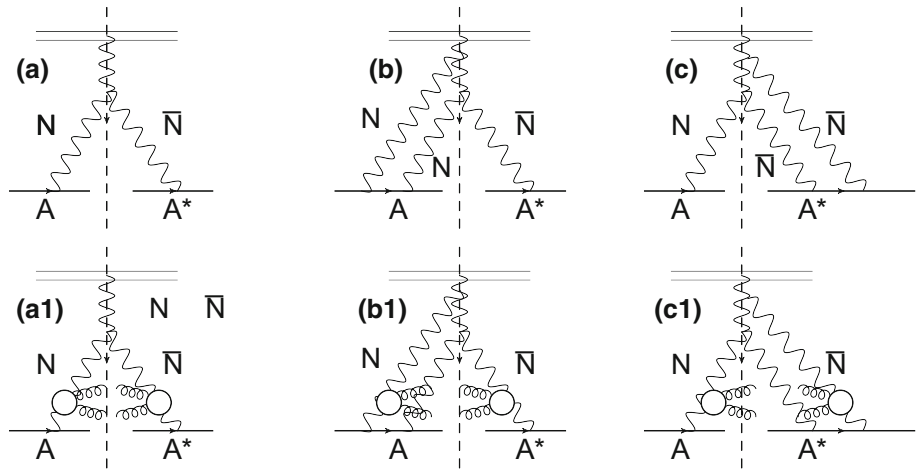


**Fig. 6** The first diagrams for  $N^D$  (a–c) and for the two gluon central diffraction productions (a1–c1)



$N^D$  denotes the cross section for diffractive production with a rapidity gap larger than  $Y_{min}$ . Generally speaking this cross section can be viewed as a product of the amplitude  $A$  and the complex conjugate amplitude  $A^*$ .  $N$  and  $\bar{N}$  are the amplitudes for elastic scattering in  $A$  and  $A^*$ , respectively. Figure 6 illustrates this notation. From this figure one can see, the difference between  $N$  and  $\bar{N}$ . For the calculation of the processes of central diffractive production, we only need to separate the diagrams of Fig. 4b2 from the other diagrams, which do not contribute to the diffraction.

The solution to Eq. (13) takes the following form

$$N^D(Y, Y_{min}) = \frac{\gamma z}{1 + \gamma(z - 1)} + \frac{\bar{\gamma} z}{1 + \bar{\gamma}(z - 1)} - \frac{\gamma + \bar{\gamma} + 2\gamma\bar{\gamma}(z_{min} - 1)}{1 - \gamma\bar{\gamma}(z_{min} - 1)^2 + (\gamma + \bar{\gamma} + 2\gamma\bar{\gamma}(z_{min} - 1))(z - 1)} \quad (14)$$

where  $z = e^{\Delta Y}$  and  $z_{min} = e^{\Delta Y_{min}}$ . Eq. (14) reduces to a more transparent expression for  $\gamma = \bar{\gamma}$ :

$$N^D(Y, Y_{min}) = \frac{2\gamma z}{1 + \gamma(z - 1)} - \frac{2\gamma z}{1 + \gamma(2z - z_{min} - 1)} \quad (15)$$

For  $z_{min} = 1$ , Eqs. (14) and (15) give the total cross section for diffraction production, which has the form:

$$N^D(Y, Y_{min}) = \frac{\gamma z}{1 + \gamma(z - 1)} + \frac{\bar{\gamma} z}{1 + \bar{\gamma}(z - 1)} - \frac{\gamma + \bar{\gamma}}{1 + (\gamma + \bar{\gamma})(z - 1)} \quad (16)$$

Using Eq. (16) we can calculate the central diffractive production cross section,<sup>2</sup> which is equal to

$$\sigma_{CD} = \Gamma^2(2IP \rightarrow 2G) \gamma \frac{\partial}{\partial \gamma} \bar{\gamma} \frac{\partial}{\partial \bar{\gamma}} N^D(Y, Y_{min}) \Big|_{\gamma=\bar{\gamma}} = \Gamma^2(2IP \rightarrow 2G) \frac{2\gamma^2 z(z - 1)}{(1 + 2\gamma(z - 1))^3} \quad (17)$$

where  $\Gamma^2(2IP \rightarrow 2G)$  denotes the vertex of two gluon production from Pomeron exchange.

### 3.2 Healing the Finkelstein–Kajantie disease

Having calculated the central diffractive production, we can shed light on an old problem which was understood in the

<sup>2</sup> Equation (17) gives the amplitude in the simplified case when there is no Pomeron interactions below the vertex  $\Gamma(2IP \rightarrow 2G)$  as one can see from Fig. 6. The general case will be considered in Sect. 3.3.

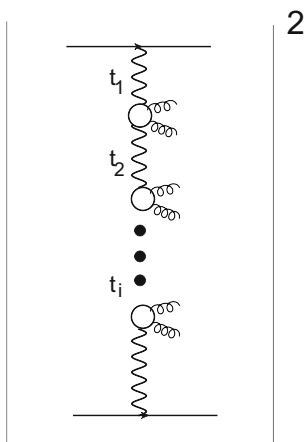


**Fig. 7** The process of multi central diffractive production due to multi Pomeron exchanges. The wavy lines describe the Pomerons

1960’s: the process of production of pairs of the gluons separated by a large rapidity gap (LRG), could violate unitarity constraints. Indeed, let us assume that the resulting Green function of the Pomeron produces an amplitude that does not depend on the energy. In this case, the production of the  $GG$  pair due to multi Pomeron exchanges, shown in Fig. 7, leads to the power-like increase of the scattering amplitude [66] (see also Refs. [67–70]). This increase occurs due to integration over the rapidities of the  $GG$  vertices, for the production of  $n$ -gluon pairs it generates the contribution which is proportional to  $(\Gamma^2(2IP \rightarrow 2G) Y)^n / n!$ . Summing over  $n$  leads to the power-like increase of the amplitude. This phenomenon was unjustifiably called the Finkelstein–Kajantie disease (see review of Ref. [68]). The widely held opinion at that time was that  $\Gamma^2(2IP \rightarrow 2G) \propto t_i$ . Such suppression, turns out to be sufficient to suppress this process at high energies. However, no reason for such a behavior has been found over almost five decades, and as we have argued, no such suppression appears in QCD for two gluon production by the Pomeron.

On the other hand, one can see that Eq. (17) leads to the cross section for central diffraction, which decreases as  $e^{-\Delta Y}$ , without any problem with unitarity. The emission of more than one pair of gluons, which is equal to

$$\sigma_{CD}^{(k)} = (\Gamma^2(2IP \rightarrow 2G))^k \left( \gamma \frac{\partial}{\partial \gamma} \bar{\gamma} \frac{\partial}{\partial \bar{\gamma}} \right)^k N^D(Y, Y_{min}) \Big|_{\gamma=\bar{\gamma}}$$

$$\xrightarrow{z \gg 1} \frac{1}{z}$$

$$= e^{-\Delta Y} \tag{18}$$

where  $k$  which denotes the number of produced pairs of gluons, does not change the behavior of the amplitude at large values of  $Y$ .

We need to compare this behavior of the scattering amplitude with the contribution of the diagram of Fig. 7, which leads to

$$A \propto e^{\Delta_{sum} Y}; \quad \text{with} \quad \Delta_{sum} = \Delta + \Gamma^2(2IP \rightarrow 2G) \tag{19}$$

In other words, the ‘fan’ diagrams of Fig. 6 generate the survival probability, which suppress both the power-like growth of the ‘bare’ Pomeron, and the increase due to the multi-Pomeron production.

Generally speaking, we showed the suppression in a rather specific model, but one can see that the amplitude  $N^D \rightarrow 1$  at large  $Y$ , and it approaches this limit as  $e^{-\Delta Y}$ :  $N^D = 1 - \mathcal{O}(e^{-\Delta Y})$ . After differentiation over  $\gamma$  and  $\bar{\gamma}$ , only the correction term remains. We will see below that this structure is preserved in QCD.

### 3.3 Generating functional for the production processes

Equation (19) resolves the FK problem, but it also shows that contribution of central diffraction turns out to be rather small. In other words, if we suggest an experiment to measure the events with multiplicity  $n \geq \bar{n}$ , we expect, at high energies, the violation of  $\phi \rightarrow \pi - \phi$  symmetry, to be small. Fortunately, for the Balitsky–Kovchegov cascade, we know how to calculate the events with different multiplicities in the BFKL Pomeron calculus in zero transverse dimension [65]. To do this, we need to introduce the generating function<sup>3</sup>

$$Z(w, \bar{w}, v; Y) = \sum_{k=0, l=0, m=0}^{\infty} P(k, l, m; Y) w^k \bar{w}^l v^m \tag{20}$$

where  $k(l)$  denotes the number of uncut Pomerons in the amplitude and in the complex conjugate amplitude, and  $m$  is the number of cut Pomerons at rapidity  $Y$ . In Ref. [65] it is shown that this generating function satisfies the following equation:

$$\frac{\partial Z(w, \bar{w}, v; Y)}{\partial \Delta Y} = - \left( w(1-w) \frac{\partial Z(w, \bar{w}, v; Y)}{\partial w} + \bar{w}(1-\bar{w}) \frac{\partial Z(w, \bar{w}, v; Y)}{\partial \bar{w}} + (2w\bar{w} - 2(w+\bar{w})v + v^2 + v) \frac{\partial Z(w, \bar{w}, v; Y)}{\partial v} \right) \tag{21}$$

The solution to this equation takes the following form

$$Z(w, \bar{w}, v; Y) = \frac{w}{(1-w)(z-1) + 1} + \frac{\bar{w}}{(1-\bar{w})(z-1) + 1} - \frac{w + \bar{w} - v}{(1-w-\bar{w}+v)(z-1) + 1} \tag{22}$$

where  $z = e^{\Delta Y}$ .

<sup>3</sup> In the general case of the BFKL Pomeron calculus in four dimensions this function will be a functional [58–61].

We can identify the scattering amplitude with  $N(\gamma, \bar{\gamma}, \gamma_{in}; Y) = 1 - Z(1 - \gamma, 1 - \bar{\gamma}, 1 - \gamma_{in}; Y)$  [55–57, 60, 65] and obtain the following expression for the amplitude:

$$N(\gamma, \bar{\gamma}, \gamma_{in}; Y) = \frac{\gamma z}{\gamma(z-1) + 1} + \frac{\bar{\gamma} z}{\bar{\gamma}(z-1) + 1} - \frac{(\gamma + \bar{\gamma} - \gamma_{in})z}{(\gamma + \bar{\gamma} - \gamma_{in})(z-1) + 1} \tag{23}$$

where  $\gamma = \bar{\gamma}$  denotes the amplitude for the elastic interaction of a single dipole with the target at  $Y = Y_0$ , while  $\gamma_{in}$  denotes the amplitude of the inelastic interaction. Due to the AGK cutting rules,  $\gamma_{in} = 2\gamma = 2\bar{\gamma}$ .

Note that Eq. (23) leads to Eq. (16) for the total cross section of diffraction production at  $\gamma_{in} = 0$ . This condition means that we do not produce even one cut Pomeron.

From Eq. (23) we can calculate the result for the total inclusive measurement. Indeed, the total cross section for central diffraction, without any selection with respect of the multiplicity of the events, is equal to

$$\sigma_{CD} = \Gamma^2(2IP \rightarrow 2G) \gamma \frac{\partial}{\partial \gamma} \bar{\gamma} \frac{\partial}{\partial \bar{\gamma}} N(\gamma, \bar{\gamma}, \gamma_{in}; Y) \Big|_{\gamma_{in}=2\gamma=2\bar{\gamma}} = \Gamma^2(2IP \rightarrow 2G) 2\gamma^2 z(z-1) \tag{24}$$

The double inclusive cross section for two cut Pomeron production which is accompanied by any number cut and uncut Pomerons is equal to

$$\sigma_{BE} = \frac{1}{N_c^2 - 1} \Gamma_G^2 \gamma_{in}^2 \frac{\partial}{\partial \gamma_{in}} \frac{\partial}{\partial \gamma_{in}} N(\gamma, \bar{\gamma}, \gamma_{in}; Y) \Big|_{\gamma_{in}=2\gamma=2\bar{\gamma}} = \frac{1}{N_c^2 - 1} \Gamma_G^2 2\gamma_{in}^2 z(z-1) \tag{25}$$

Equation (25) describe the Bose–Einstein interference diagram and the contribution for the entire inclusive measurement with  $\Gamma_G$  being the Mueller vertex for the inclusive production of one gluon.

One can see that for

$$\Gamma^2(2IP \rightarrow 2G) = \frac{4}{N_c^2 - 1} \Gamma_G^2 \tag{26}$$

$\sigma_{BE} = \sigma_{CD}$ , which results in the symmetry  $\phi \rightarrow \pi - \phi$ .

The contribution to the correlation function of the even  $n$  with fixed multiplicity :  $n = k\bar{n}$ , is given by the following formula:

$$\begin{aligned} \sigma_n^{BE} &= \frac{1}{N_c^2 - 1} \Gamma_G^2 \frac{\gamma_{in}^k}{k!} \frac{\partial}{\partial \gamma_{in}^k} N(\gamma, \bar{\gamma}, \gamma_{in}; Y) \Big|_{\gamma_{in}=0, \gamma=\bar{\gamma}} \\ &= \frac{1}{N_c^2 - 1} \Gamma_G^2 \gamma_{in}^k \frac{z(z-1)^{k-1}}{(1+2\gamma(z-1))^{k+1}} \\ &= \frac{1}{N_c^2 - 1} \Gamma_G^2 (2\gamma)^k \frac{z(z-1)^{k-1}}{(1+2\gamma(z-1))^{k+1}} \end{aligned} \tag{27}$$

The cross section for central diffraction with the same multiplicity of produced gluons takes the form:

$$\begin{aligned} \sigma_n^{CD} &= \Gamma^2(2IP \rightarrow 2G) \gamma \frac{\partial}{\partial \gamma} \bar{\gamma} \frac{\partial}{\partial \bar{\gamma}} \frac{\gamma_{in}^k}{k!} \frac{\partial}{\partial \gamma_{in}^k} N(\gamma, \bar{\gamma}, \gamma_{in}; Y) \Big|_{\gamma_{in}=0, \gamma=\bar{\gamma}} \\ &= (k+2)(k+1) \Gamma^2(2IP \rightarrow 2G) \gamma^2 \gamma_{in}^k \frac{z(z-1)^{k+1}}{(1+2\gamma(z-1))^{k+3}} \\ &= (k+2)(k+1) \Gamma^2(2IP \rightarrow 2G) \gamma^2 (2\gamma)^k \frac{z(z-1)^{k+1}}{(1+2\gamma(z-1))^{k+3}} \end{aligned} \tag{28}$$

However, the simple formulae of Eqs. (27) and (28) are only correct, if we do not fix the rapidity of the emitted particles. Indeed, if the emitted gluons have rapidity  $y_1 \approx y_2 = \frac{1}{2}Y$ , we have to calculate  $\sigma_n^{BE}$  and  $\sigma_n^{CD}$  using Eqs. (27) and (28) for rapidity  $\frac{1}{2}Y$  and insert in this formulae  $\gamma = \bar{\gamma} = \frac{\gamma z}{\gamma(z-1)+1}$  with  $z = \exp(\frac{1}{2}\Delta Y)$  (see Fig. 8a). For example  $\sigma_0^{CD}$  takes the form

$$\begin{aligned} \sigma_0^{CD} &= \Gamma^2(2IP \rightarrow 2G) \\ &\times \gamma \frac{\partial}{\partial \gamma} \bar{\gamma} \frac{\partial}{\partial \bar{\gamma}} N\left(\gamma, \bar{\gamma}, \gamma_{in}; \frac{1}{2}Y\right) \Big|_{\gamma_{in}=0, \gamma=\bar{\gamma}} = \frac{\gamma \exp(\frac{1}{2}\Delta Y)}{1+\gamma(\exp(\frac{1}{2}\Delta Y)-1)} \\ &= 2\Gamma^2(2IP \rightarrow 2G) \frac{(\gamma e^{\Delta Y})^2 (1 + \gamma e^{\frac{1}{2}\Delta Y})}{(1 + \gamma (2e^{\Delta Y} - e^{\frac{1}{2}\Delta Y}))^3} \end{aligned} \tag{29}$$

where  $\gamma$  denotes the dipole amplitude at  $Y = Y_0$ , and we assumed that  $\exp(\frac{1}{2}\Delta Y) \gg 1$ .

We need to find the scattering amplitude with one cut Pomeron, which is equal to

$$\begin{aligned} A(1 \text{ cut Pomeron}, Y) &= \gamma_{in} \left( \frac{\partial}{\partial \gamma_{in}} N(\gamma, \bar{\gamma}, \gamma_{in}; Y) \Big|_{\gamma_{in}=0, \gamma=\bar{\gamma}} \right) \\ &= \frac{2\gamma e^{\Delta Y}}{(1 + 2\gamma(e^{\Delta Y} - ))^2} \end{aligned} \tag{30}$$

Using Eq. (30) we obtain

$$\begin{aligned} \sigma_1^{CD} &= \Gamma^2(2IP \rightarrow 2G) A(1 \text{ cut Pomeron}, \frac{1}{2}Y) \\ &\times \frac{\partial}{\partial \gamma_{in}} \left( \gamma \frac{\partial}{\partial \gamma} \bar{\gamma} \frac{\partial}{\partial \bar{\gamma}} N\left(\gamma, \bar{\gamma}, \gamma_{in}; \frac{1}{2}Y\right) \right) \Big|_{\gamma_{in}=0, \gamma=\bar{\gamma}} = \frac{\gamma \exp(\frac{1}{2}\Delta Y)}{1+\gamma(\exp(\frac{1}{2}\Delta Y)-1)} \\ &= 12 \Gamma^2(2IP \rightarrow 2G) \\ &\times \frac{(\gamma e^{\Delta Y})^3 (1 + \gamma e^{\frac{1}{2}\Delta Y})^2}{(1 + 2\gamma e^{\frac{1}{2}\Delta Y})^2 (1 + \gamma (2e^{\Delta Y} - e^{\frac{1}{2}\Delta Y}))^4} \end{aligned} \tag{31}$$

We also need to take into account the events with multiplicities less than  $\bar{n}$ , which stem from the processes of diffraction dissociation. For this we need to replace in Eq. (31)  $A(1 \text{ cut Pomeron}, \frac{1}{2}Y)$  with the amplitude of the cross section of the diffraction production  $N(\gamma, \gamma, 0, Y)$ . In Fig. 8c

**Fig. 8** Graphic forms of  $\sigma_0^{CD}$  (a) and  $\sigma_1^{CD}$  (b). The dotted line show the cut Pomerons

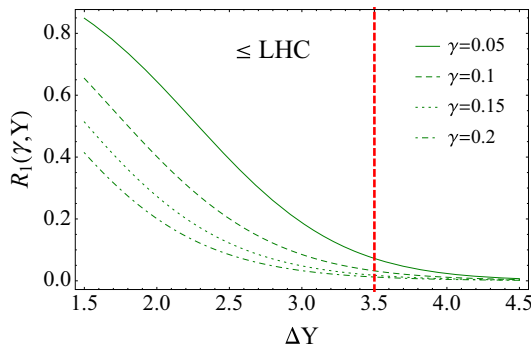
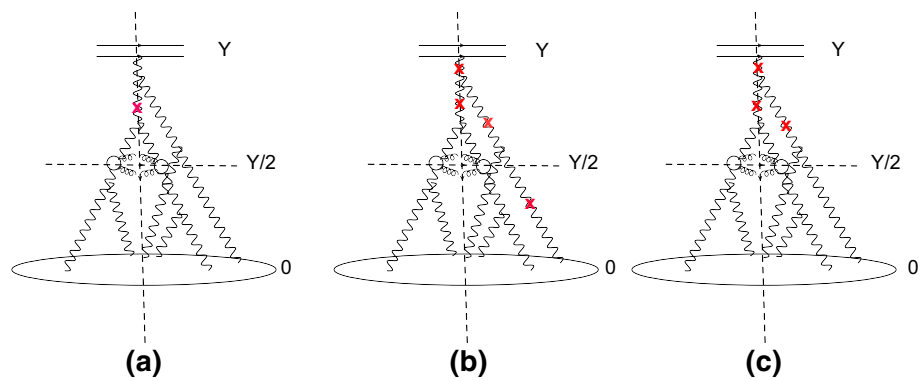


**Fig. 9** The damping factor  $R_1$  versus  $\Delta Y$  for different values of the amplitude  $\gamma$  at  $Y = Y_{\min}$

we show an example of such processes. We denoted the cross section for such processes by  $\sigma_{\frac{1}{2}}^{CD}$ .

Introducing the damping factor  $R_1$  as

$$R_1(\gamma, \Delta Y) = \frac{\sigma_0^{CD} + \sigma_1^{CD} + \sigma_{\frac{1}{2}}^{CD}}{\sum_{n=0}^{\infty} \sigma^{CD}} \quad (32)$$

Note that the value of  $R_1$  depends crucially on the values of the amplitude  $\gamma$  and of the Pomeron intercept  $\Delta$ . For DIS this amplitude is proportional to  $\tilde{\alpha}_S^2$  and we expect that it is small. The value of  $\Delta$  in DIS is a function of the value of  $Q$ . It changes from  $\Delta = 0.1$  for  $Q \sim 1 \text{ GeV}$  to  $\Delta = 0.3$  at  $Q = 10 \text{ GeV}$ . For the estimates in the kinematic region of the LHC, we took  $\Delta = 0.2$  (Fig. 9).

In the next section we consider a more realistic approach to determine these parameters. In Fig. 10 we compare  $\sigma_n^{BE}$  and  $\sigma_n^{CD}$  for the events with fixed multiplicities:  $n = k\bar{n}$ , where  $\bar{n}$  denotes the average multiplicity. One can see that for different values of  $k$  and at different rapidities, we have different relations between central diffraction production and Bose–Einstein enhancement.

### 3.4 Schwimmer model for hadron–nucleus scattering with induced $\phi \rightarrow \pi - \phi$ symmetry: $v_{n,n}$ and $v_n$

In the previous sections we discussed the BFKL Pomeron calculus in zero transverse dimension as a simplified model for the QCD cascade. However, it was noted long ago [71] that this type of model, is the correct approach to the hadron–nucleus interaction in the soft Pomeron calculus, with a triple Pomeron interaction. Indeed, the soft Pomeron, generally speaking, has a trajectory  $\alpha_P(t) = 1 + \Delta + \alpha'_P t$ , but  $\alpha'_P \ln(s/s_0)$  turns out to be smaller than  $R_A^2$  ( $\alpha'_P \ln(s/s_0) \ll R_A^2$  for all accessible energies, and, therefore, it can be neglected. Since the vertex  $G_{3P}$  is small, we can neglect the contribution of the Pomeron loops which are proportional to  $G_{3P}^2$ , and consider only ‘fan’ diagrams (see examples of these diagrams in Fig. 6a–c) which are of the order of  $(G_{3P} g S_A(b))^k$ , where  $k$  denotes the number of Pomerons,  $g$  the strength of the vertex of the Pomeron–nucleon interaction and  $S_A(b)$  is given by

$$S_A(b) = \int_{-\infty}^{+\infty} dz \rho(\sqrt{z^2 + b^2}) \quad \text{with} \quad \int d^2b S_A(b) = A \quad (33)$$

$b$  denotes the impact parameter of the nucleon and  $\rho$  the density of the nucleons in the nucleus.

Bearing this in mind, the general Eq. (23) can be rewritten replacing  $\gamma = \bar{\gamma}$  by  $G_{3P} g S_A(b) / (2\Delta)$  (see Refs. [63,64].<sup>4</sup>) We suggest the following strategy to find  $G_{3P}$  from the experimental data on soft interactions:

$$G_{3P} g = \frac{1}{2} \frac{\sigma_{\text{dif}}^{\text{HM}}}{\sigma_{el}} \quad (34)$$

In Eq. (34) we assumed, that both elastic and single diffraction can be described as the exchange of two Pomerons, and that the  $t$  dependence of the triple Pomeron vertex can be neglected in comparison with the elastic slope. It should

<sup>4</sup> In these references the Schwimmer approach of Ref. [71] was generalized for the intercept of the Pomeron  $\Delta_P > 0$ .

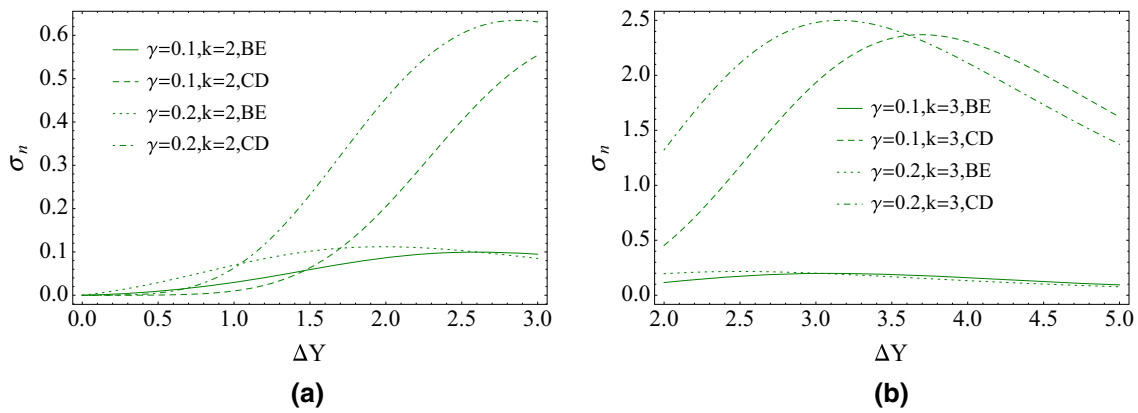


**Fig. 10**  $\sigma_n^{BE}$  and  $\sigma_n^{CD}$  with the multiplicity of the produced gluons equal to  $n = k\bar{n}$  versus  $Y$

be noted that both assumptions are in agreement with high energy phenomenology (see for example Ref. [72]). The value of the cross section for diffractive production in the region of high mass  $\sigma_{dif}^{HM}$  is taken from Ref. [72]. From Eq. (34) we see that the parameter  $G_{3IP}gz$  which enters Eqs. (27) and (28) can be written as

$$s_{pp} \equiv G_{3IP}gz = \left(\frac{1}{2} \frac{\sigma_{dif}^{HM}}{\sigma_{el}}\right) \sigma_{in} \tag{35}$$

where  $\sigma_{in}$  denotes the inelastic cross section for proton-proton interaction at high energy. Considering  $z \gg 1$  we can re-write Eqs. (27) and (28) in terms of  $s_{pp}$  in the form:

$$\sigma_n^{BE} = \frac{1}{N_c^2 - 1} \Gamma_G^2 \frac{(2s_{pp} S_A(b))^k}{(1 + 2s_{pp} S_A(b))^{k+1}}; \tag{36}$$

$$\sigma_n^{CD} = \frac{(k+2)(k+1)}{4} \Gamma^2 (2IP \rightarrow 2G) \times \frac{(2s_{pp} S_A(b))^{k+2}}{(1 + 2s_{pp} S_A(b))^{k+3}} \tag{37}$$

Using these equations, we can estimate the contribution to the double inclusive production of the terms which violate  $\phi \rightarrow \pi - \phi$  symmetry, due to selections of the events with restricted multiplicities. If we select all events with multiplicity  $n \geq 2\bar{n}$ , where  $\bar{n}$  is the average multiplicity, the central diffraction production with multiplicities  $n < 2\bar{n}$  will be not measured and, therefore, has to be subtracted from the inclusive measurements that show the  $\phi \rightarrow \pi - \phi$  symmetry. We can introduce the parameters

$$R_1(W) = \frac{\sigma_0^{CD} + \sigma_1^{CD}}{\sum_{n=0}^{\infty} \sigma_n^{CD}}; \tag{38}$$

$$R_0(W) = \frac{\sigma_0^{CD}}{\sum_{n=0}^{\infty} \sigma_n^{CD}};$$

whose values show the suppression of the symmetry violation terms, with respect to symmetry preserving one.  $R_1$  characterizes the violation of the symmetry in the measurement

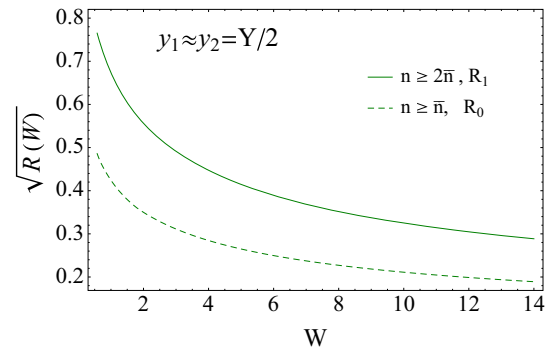


**Fig. 11**  $R_1$  and  $R_0$  versus energy  $W$  for proton-gold scattering for  $y_1 \approx y_2 = \frac{1}{2}Y$

with the multiplicity  $n \geq 2\bar{n}$ , while  $R_0$  shows this violation for the measurements with large multiplicity  $n \geq \bar{n}$ .

Figure 11 shows the value of these parameters in the Schwimmer model with the parameters that are found using Eqs. (33) and (34). In Fig. 11 we plot the result of the estimates from Eqs. (29) and (31) fixing  $y_1 \approx y_2 = \frac{1}{2}Y$ . For making such estimates we parametrized Eq. (34) as  $s_{pp} = 0.025 \exp(0.2Y)$ .

Using  $R$  we can express  $v_{n,n}$  and  $v_n$  through the harmonics that has been evaluated from the Bose–Einstein correlations [18–20]. Indeed, it turns out that

$$v_{2n,2n} = (2 - R) v_{2n,2n}^{BE}; \quad v_{2n-1,2n-1} = R v_{2n-1,2n-1}^{BE};$$

$$v_{2n} = \sqrt{2 - R} v_{2n}^{BE};$$

$$v_{2n-1} = \sqrt{R} v_{2n-1}^{BE}; \tag{39}$$

One can see from Fig. 11 ( see Eqs. (36) and (37) that the odd harmonics are small at high energies but they are sizable at  $W = 5.5TeV$  since  $\sqrt{R_1} = 0.32$  and  $\sqrt{R_0} = 0.25$  at this energy. Recall, that at the moment, this is the highest energy available for hadron–nucleus scattering data.

### 4 QCD cascade

In the previous section we discussed the simplified model which actually reproduces only two features of the CGC/saturation approach: the form of Eq. (10) and the relation given by Eq. (26). In this section we wish to repeat the previous estimates on more general grounds of high energy QCD. However, it should be stressed that the longitudinal structure of the QCD cascade, is very close to that of the model, that we have considered. In particular, we can introduce the generating functional [73]

$$\begin{aligned}
 & Z(\{w(r_k)\}, \{\bar{w}(r_l)\}, \{v(r_m)\}; Y) \\
 &= \sum_{k=0, l=0, m=0}^{\infty} P_{k,l}^m(r_1, \dots, r_k; r_1, \dots, r_l; r_1, \dots, r_m; Y) \prod_{i=0}^k w(r_i) \\
 &\quad \times \prod_{i=0}^l \bar{w}(r_i) \prod_{i=0}^m v(r_i) \tag{40}
 \end{aligned}$$

where  $w(r_i)$ ,  $\bar{w}(r_i)$  and  $v(r_i)$  are arbitrary functions and  $P_{k,l}^m$  is the probability to have  $k$  and  $l$  dipoles with the coordinates  $r_i$  in uncut Pomerons, while  $m$  is the number of dipoles in the cut Pomerons at rapidity  $Y$ . For this functional, we can write the functional linear equations which are similar to the ones in the simplified model (see Ref. [73] for details). Bearing these general features in mind, we suggest a simpler approach which is based on the non-linear Balitsky–Kovchegov equation [55–57], and on general properties of the solution, that we have discussed above in the simplified model.

#### 4.1 The simplified non-linear equation

The simplified version of the Balitsky–Kovchegov (BK) equation was proposed in Ref. [74] and has been discussed in detail in Refs. [75, 76]. Here we give a brief review of this equation and concentrate our efforts on finding the solution in the form which can be used for calculating the angular correlations. The BK equation takes the following form:

$$\begin{aligned}
 & \frac{\partial N(Y; \mathbf{x}_{01}, \mathbf{b})}{\partial Y} \\
 &= \frac{\bar{\alpha}_S}{2\pi} \int d^2\mathbf{x}_2 K(\mathbf{x}_{01}; \mathbf{x}_{02}, \mathbf{x}_{12}) \left\{ N\left(Y; \mathbf{x}_{02}, \mathbf{b} - \frac{1}{2}\mathbf{x}_{12}\right) \right. \\
 &+ N\left(Y; \mathbf{x}_{12}, \mathbf{b} - \frac{1}{2}\mathbf{x}_{02}\right) - N(Y; \mathbf{x}_{01}, \mathbf{b}) \\
 &\left. - N\left(Y; \mathbf{x}_{02}, \mathbf{b} - \frac{1}{2}\mathbf{x}_{12}\right) N\left(Y; \mathbf{x}_{12}, \mathbf{b} - \frac{1}{2}\mathbf{x}_{02}\right) \right\} \quad \text{where} \\
 & K(\mathbf{x}_{01}; \mathbf{x}_{02}, \mathbf{x}_{12}) = \frac{\mathbf{x}_{01}^2}{\mathbf{x}_{02}^2 \mathbf{x}_{12}^2} \tag{41}
 \end{aligned}$$

where  $N(Y; \mathbf{x}_{01}, \mathbf{b})$  denotes the dipole scattering amplitude.

Since the analytical solution to Eq. (41) has not been found, in Ref. [74] it was suggested to simplify the kernel by taking into account only log contributions. We have

two kinds of logs:  $\left(\bar{\alpha}_S \ln\left(x_{01}^2 \Lambda_{QCD}^2\right)\right)^n$  in the perturbative QCD kinematic region where  $x_{01}^2 Q_s^2(Y, b) \equiv \tau \ll 1$ ; and  $\left(\bar{\alpha}_S \ln\left(x_{01}^2 Q_s^2(Y, b)\right)\right)^n$  inside the saturation domain ( $\tau \gg 1$ ), where  $Q_s(Y, b)$  is the saturation scale. To sum these logs we need to modify the BFKL kernel in different ways in the two kinematic regions. From the formal point of view, this simplification means that we consider only the leading twist contribution to the BFKL kernel, which includes all twist contributions in the form of Eq. (41). For the perturbative QCD region of  $\tau \ll 1$ , the logs originate from  $x_{02}^2 \sim x_{12}^2 \ll x_{01}^2$  resulting in the following form of the kernel  $K(\mathbf{x}_{01}; \mathbf{x}_{02}, \mathbf{x}_{12})$  [74]

$$\int d^2x_{02} K(\mathbf{x}_{01}; \mathbf{x}_{02}, \mathbf{x}_{12}) \rightarrow \pi x_{01}^2 \int_{r^2}^{\frac{1}{\Lambda_{QCD}^2}} \frac{dx_{02}^2}{x_{02}^4} \tag{42}$$

The non-linear BK equation in this region can be written as

$$\begin{aligned}
 & \frac{\partial^2 n(Y; \mathbf{x}_{01}, \mathbf{b})}{\partial Y \partial \ln\left(1/(x_{01}^2 \Lambda_{QCD}^2)\right)} \\
 &= \frac{\bar{\alpha}_S}{2} \left( 2n(Y; \mathbf{x}_{01}, \mathbf{b}) - n^2(Y; \mathbf{x}_{01}, \mathbf{b}) \right) \tag{43}
 \end{aligned}$$

for  $n(Y; \mathbf{x}_{01}, \mathbf{b}) = N(Y; \mathbf{x}_{01}, \mathbf{b})/x_{01}^2$ .

Inside of the saturation region where  $\tau > 1$  the logs originate from the decay of a large size dipole into one small size dipole and one large size dipole. However, the size of the small dipole is still larger than  $1/Q_s$ . This observation can be translated in the following form of the kernel

$$\begin{aligned}
 & \int K(\mathbf{x}_{01}; \mathbf{x}_{02}, \mathbf{x}_{12}) d^2x_{02} \rightarrow \pi \int_{1/Q_s^2(Y, b)}^{x_{01}^2} \frac{dx_{02}^2}{x_{02}^2} \\
 &+ \pi \int_{1/Q_s^2(Y, b)}^{x_{01}^2} \frac{d|\mathbf{x}_{01} - \mathbf{x}_{02}|^2}{|\mathbf{x}_{01} - \mathbf{x}_{02}|^2} \tag{44}
 \end{aligned}$$

Inside the saturation region the BK equation takes the form

$$\begin{aligned}
 & \frac{\partial^2 \tilde{N}(Y; \mathbf{x}_{01}, \mathbf{b})}{\partial Y \partial \ln r^2} \\
 &= \bar{\alpha}_S \left\{ \left( 1 - \frac{\partial \tilde{N}(Y; \mathbf{x}_{01}, \mathbf{b})}{\partial \ln x_{01}^2} \right) \tilde{N}(Y; \mathbf{x}_{01}, \mathbf{b}) \right\} \tag{45}
 \end{aligned}$$

where  $\tilde{N}(Y; \mathbf{x}_{01}, \mathbf{b}) = \int^{x_{01}^2} dx_{02}^2 N(Y; \mathbf{x}_{02}, \mathbf{b})/x_{01}^2$ .

The new kernel in the anomalous dimension representation has the form:

$$\chi(\gamma) = \begin{cases} \frac{1}{\gamma} & \text{for } \tau \geq 1; \\ \frac{1}{1-\gamma} & \text{for } \tau \leq 1; \end{cases} \tag{46}$$

This should be compared with the full BFKL kernel in the Mellin transform:

$$\chi(\gamma) = \int \frac{d\xi}{2\pi i} e^{-\gamma\xi} K(\mathbf{x}_{01}; \mathbf{x}_{02}, \mathbf{x}_{12}),$$

$$= 2\psi(1) - \psi(\gamma) - \psi(1 - \gamma) \tag{47}$$

where  $\xi = \ln(x_{01}^2/x_{02}^2)$  and  $\psi(z) = d \ln \Gamma(z)/dz$  with  $\Gamma(z)$  equal to Euler gamma function.

One can see that the advantage of the simplified kernel of Eq. (46) is that, in Double Log Approximation (DLA) for  $\tau < 1$ , it provides a matching with the DGLAP evolution equation [77–79].

### 4.2 Solution

#### 4.2.1 Perturbative QCD region ( $\tau < 1$ )

For  $\tau = x_{01}^2 Q_s^2(Y, b) < 1$ , we can neglect the non-linear term in Eq. (43). The equation leads to the DLA solution that has the form

$$N(Y; x_{01}, b) = N_0 \exp\left(\sqrt{-\xi_s \xi} + \xi\right)$$

$$\xrightarrow{\tau \rightarrow 1; \zeta \rightarrow 0_-} N_0 e^{\frac{1}{2}\zeta} \exp\left(-\frac{\zeta^2}{8\xi_s}\right) \tag{48}$$

where we use the following notations:

$$\xi_s = 4\bar{\alpha}_S(Y - Y_{\min}); \quad \xi = \ln(x_{01}^2 Q_s^2(Y = Y_{\min}; b));$$

$$\zeta = \xi_s + \xi; \tag{49}$$

The solution of Eq. (48) provides the boundary condition for the solution inside the saturation region:

$$\frac{\partial \ln N(Y; \zeta = 0_-, (\xi = -\xi_s), b)}{\partial \zeta} = \frac{1}{2}$$

$$\partial \zeta = \frac{1}{2}; \tag{50}$$

As was expected, in the vicinity of the saturation scale ( $\zeta \ll 8\xi_s$ ), the amplitude shows geometric scaling behavior, being a function of only one variable  $\zeta$  [80–82],

$$N(Y; r, b) \propto \left(r^2 Q_s^2(Y, b)\right)^{1-\gamma_{cr}} \tag{51}$$

where  $\gamma_{cr}$  the critical anomalous dimension is equal to  $\frac{1}{2}$ .

#### 4.2.2 Saturation region ( $\tau > 1$ )

In this region we look for a solution in the form [74]

$$\tilde{N} = \int_{\xi_s}^{\xi} d\xi' \left(1 - e^{-\phi(\xi', Y)}\right) \tag{52}$$

Substituting Eq. (52) into Eq. (45) we obtain

$$\phi'_Y e^{-\phi} = \bar{\alpha}_S \tilde{N} e^{-\phi} \tag{53}$$

Canceling  $e^{-\phi}$  and differentiating with respect to  $\xi$  we obtain the equation in the form:

$$\frac{\partial^2 \phi}{\partial Y \partial \xi} = \bar{\alpha}_S \left(1 - e^{-\phi(Y; \xi)}\right) \tag{54}$$

Using variable  $\xi_s$  and  $\xi$  we can rewrite Eq. (53) in the form

$$\frac{\partial^2 \phi}{\partial \xi_s \partial \xi} = \frac{1}{4} \left(1 - e^{-\phi(Y; \xi)}\right) \text{ or in the form}$$

$$\frac{\partial^2 \phi}{\partial \zeta^2} - \frac{\partial^2 \phi}{\partial x^2} = \frac{1}{4} \left(1 - e^{-\phi(Y; \xi)}\right) \tag{55}$$

with  $\zeta$  defined in Eq. (49) and  $x = \xi_s - \xi$ .

Equation (55) has a general traveling wave solution (see Ref. [83] formula 3.4.1)

$$\int_{\phi_0}^{\phi} \frac{d\phi'}{\sqrt{c + \frac{1}{2(\lambda^2 - \kappa^2)}(\phi' - 1 + e^{-\phi'})}} = \kappa x + \lambda \zeta \tag{56}$$

where  $c, \phi_0, \lambda$  and  $\kappa$  are arbitrary constants that should be determined from the initial and boundary conditions.

From the matching with the perturbative QCD region (see Eq. (50)) we have the following initial conditions for small values of  $\phi_0$ :

$$\phi(t \equiv \zeta = 0, x) = \phi_0(b); \quad \phi'_\zeta(t \equiv \zeta = 0, x)$$

$$= \frac{1}{2} \phi_0(b) \tag{57}$$

These conditions allow us to find that  $\kappa = 0$  and  $c = 0$  for  $\phi_0 \ll 1$ . Therefore, the solution of Eq. (56) leads to geometric scaling as it depends only on one variable:  $z$ . For small values of  $\phi_0$ , it takes the form [74, 83].

$$\sqrt{2} \int_{\phi_0}^{\phi} \frac{d\phi'}{\sqrt{\phi' - 1 + e^{-\phi'}}} = \zeta \tag{58}$$

### 4.3 Formulation of the problem

The previous sections give a brief review of the simple approach to the QCD cascade of one dipole which interacts with a target. In Fig. 12a one can see the two distinct kinematic regions which we have considered above: the perturbative QCD region with  $\tau < 1$ , and the saturation domain for which  $\tau > 1$ . The key physics idea of the description of DIS with a target nucleus and/or hadron-nucleus collisions in the framework of the CGC/saturation approach, is that the physics in the saturation region is determined by the new dimensional parameter: the saturation scale, and if it is a dilute system of partons, it does not depend on the detailed structure of the projectile. In DIS we have a dipole of size  $r \sim 1/Q$ . For the hadron-nucleus collision we identify the projectile hadron with a dipole of the same size. In these processes we have two different situations which are shown in Fig. 12-a and Fig. 12b. For small dipoles

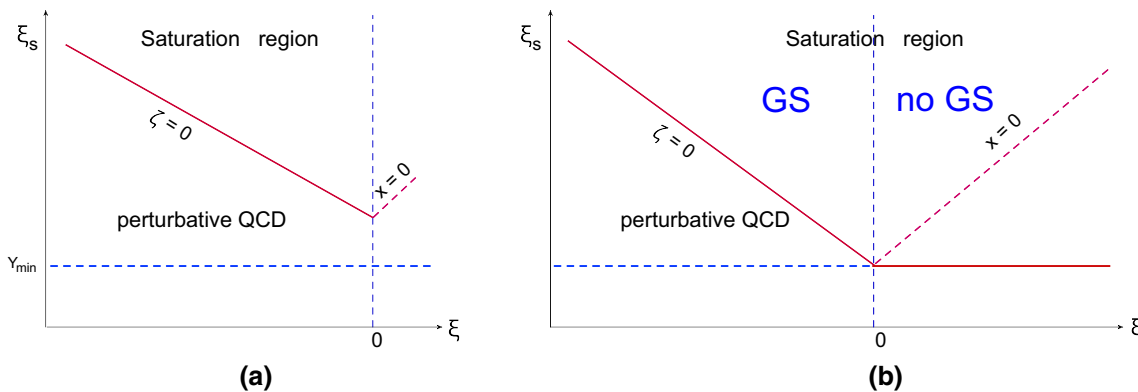


**Fig. 12** QCD map. **a** shows the kinematic regions for the case when  $N(Y = Y_{\min}, \xi) \ll 1$  while in **b** we show the kinematic regions for  $N(Y = Y_{\min}, \xi) \sim 1$  (see Ref. [76] for more details). Note that the

saturation domain in this case can be divided in two subregions: (i) for  $\xi < 0$ , where we expect the geometric scaling behaviour of the scattering amplitude, and  $\xi > 0$  where there is no such behaviour

$\tau_m \equiv r^2 Q_s^2(A; Y_{\min}; b) \ll 1$ , we have  $N(Y_{\min}, r, b) \ll 1$  and the amplitude reaches the saturation region due the BFKL evolution (see Fig. 12a). For such dipoles we can safely use the solution of Eq. (58) which we have discussed above.

If the size of the dipole is large and  $\tau_m \geq 1$ , we have to deal with the situation shown in Fig. 12b, and we will discuss this case later.

In the CGC/saturation approach the initial condition for the scattering amplitude is given by the McLerran-Venugopalan (MV) formula [88–91]:

$$N_A(r^2; Y; b) = 1 - 1 - \exp(-r^2 Q_s^2(A; Y = Y_{\min})) = 1 - e^{-\tau_m} \tag{59}$$

where  $Q_s(A; Y = Y_{\min})$  is the saturation momentum at the initial energy. For the moment we consider the case of small  $\tau_m$ , and replace Eq. (59) by  $N_A(r^2; Y; b) = \tau_m$ .

For hadron–nucleus scattering the initial condition can be taken from the non-perturbative approach, or from the high energy phenomenology. For obvious reasons we have to use phenomenology which we have discussed in Sect. 3.4. We found the value of the amplitude at  $W = 0.576 \text{ GeV}$  at  $b = 0$  is equal to 0.7. To obtain the value at  $Y = Y_{\min}$ , we need to know the energy dependence of the amplitude, which can be obtained from high energy phenomenology. In most attempts to build such a phenomenology, the behaviour of the cross section with energy are assumed to be Reggeon-like,  $A \propto s^\Delta$  with  $\Delta \geq 0.14$ . In our own approach[84–86] the value of  $\Delta \approx 0.25$ , but even a value of  $\Delta = 0.14$  leads to the amplitude at  $Y = Y_{\min}$  equal to 0.12 (0.3 for our model). Therefore, it appears reasonable to assume that we have a situation which is shown in Fig. 12a. However, we will also consider the alternative situation which is related to Fig. 12b.

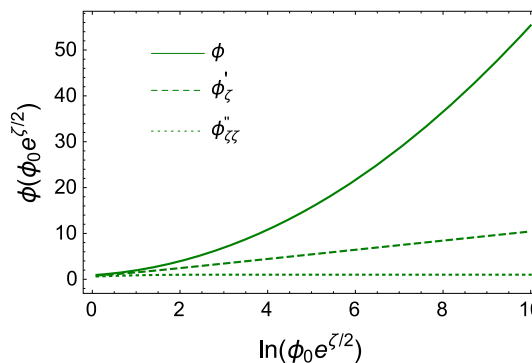


**Fig. 13** The solution to Eq. (60) for functions  $\phi(\zeta)$ ,  $d\phi(\zeta)/d\zeta$  and  $d^2\phi(\zeta)/d\zeta^2$

#### 4.4 Processes with different multiplicities of produced gluons for $\tau_m \ll 1$

Rewriting Eq. (58) in the form

$$\frac{1}{\sqrt{2}} \int_{\phi_0}^{\phi} \frac{d\phi'}{\sqrt{\phi' - 1 + e^{-\phi'}}} + \ln \phi_0 = \ln \phi_0 + \frac{1}{2}\zeta = \ln(\phi_0 e^{\frac{1}{2}\zeta}) \tag{60}$$

we can find the solution to the equation as function of  $\phi_0 e^{\frac{1}{2}\zeta}$ :  $\phi(\phi_0 e^{\frac{1}{2}\zeta})$ . Practically, the left hand side of Eq. (60) does not depend on the value of  $\phi_0$ .

This function is shown in Fig. 13.

We suggest using the following expression for the amplitude  $N(\gamma, \bar{\gamma}, \gamma_{in}; \zeta)$

$$N(\gamma, \bar{\gamma}, \gamma_{in}; \zeta) = 1 - e^{-\phi(\gamma e^{\frac{1}{2}\zeta})} - e^{-\phi(\bar{\gamma} e^{\frac{1}{2}\zeta})} + e^{-\phi((\gamma + \bar{\gamma} - \gamma_{in}) e^{\frac{1}{2}\zeta})} \tag{61}$$

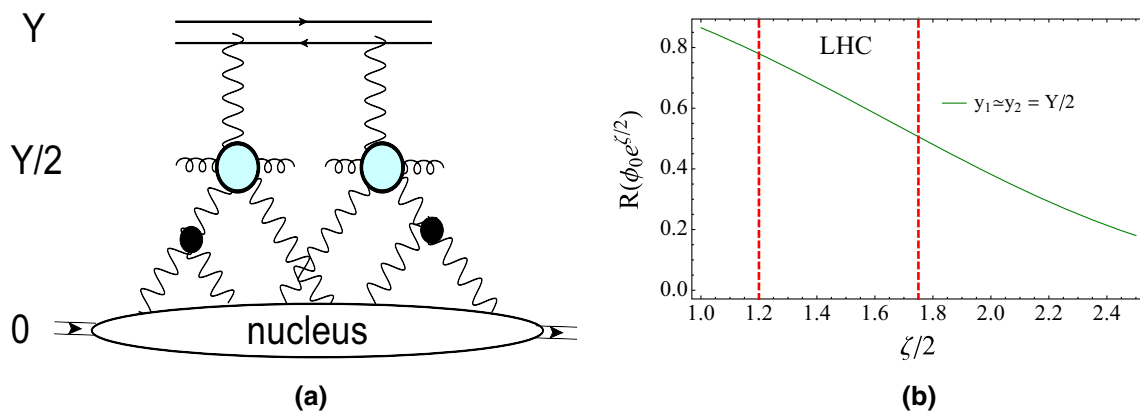


**Fig. 14** **a** The Mueller diagram for the Bose–Einstein correlation function with  $y_1 = y_2 = \frac{1}{2}Y$ . **b** The suppression factor  $R$  of Eq. (64) as function of  $\zeta$ . The vertical dotted lines show the LHC kinematic region

From Eq. (61) for the amplitude we can estimate the central diffraction production with multiplicity  $n < 2\bar{n}$  using Eq. (24). We can use simplifications, as it turns out that  $\phi'_\zeta \gg \phi''_{\zeta}$  (see Fig. 13). The cross section for central diffraction with multiplicity  $n < 2\bar{n}$  is equal to  $\sigma_0^{\text{CD}} + \sigma_1^{\text{CD}}$  and can be estimated as follows:

$$\begin{aligned} \sigma_0^{\text{CD}} + \sigma_1^{\text{CD}} &= \frac{1}{4}\Gamma^2(2P \rightarrow 2G) \left\{ \phi_\zeta'^2 + \frac{\gamma_{\text{in}}}{2\gamma} \phi_\zeta'^3 \right\} e^{-\phi(2\gamma e^{\frac{1}{2}\zeta})} \\ &= \frac{1}{4}\Gamma^2(2P \rightarrow 2G) \left\{ \phi_\zeta'^2 + \phi_\zeta'^3 \right\} e^{-\phi(2\gamma e^{\frac{1}{2}\zeta})} \end{aligned} \quad (62)$$

We assume that  $\gamma_{\text{in}} = 2\gamma$ , since the amplitude in the perturbative QCD region is due to the exchange of the BFKL Pomeron, which has this property. The Bose–Einstein correlation can be evaluated using the diagram of Fig. 14.

The contribution of this diagram has the form [48]:

$$\sigma^{\text{BE}} = \frac{1}{N_\zeta^2 - 1} \Gamma_G^2 \left( \phi_0 e^{\frac{1}{2}(\zeta - \frac{1}{2}\zeta)} \right)^2 \left( 1 - e^{-2\phi(\phi_0 e^{\frac{1}{4}\zeta})} \right)^2 \quad (63)$$

Finally the suppression factor  $R$  is equal to

$$\begin{aligned} R(\phi_0 e^{\frac{1}{2}\zeta}) &= \frac{\sigma_0^{\text{CD}} + \sigma_1^{\text{CD}}}{\sigma^{\text{BE}}} \\ &= \left\{ \phi_\zeta'^2 + \phi_\zeta'^3 \right\} e^{-\phi(2\phi_0 e^{\frac{1}{2}\zeta})} / \left( \phi_0 e^{\frac{1}{2}(\zeta - \frac{1}{2}\zeta)} \right)^2 \\ &\quad \times \left( 1 - e^{-2\phi(\phi_0 e^{\frac{1}{4}\zeta})} \right)^2 \end{aligned} \quad (64)$$

In Eq. (64) we did not fix the value of  $y_1 \approx y_2$ . The curve in Fig. 14-b is calculated for  $y_1 \approx y_2 = \frac{1}{2}Y$ . The difference occurs since for these estimates the argument  $\phi_0 \exp(\frac{1}{2}\zeta)$  of  $\phi$  in  $\sigma_0^{\text{CD}} + \sigma_1^{\text{CD}}$  should be replaced by  $\phi(\ln(\phi(\phi_0 \exp(\frac{1}{4}\zeta))) + \frac{1}{4}\zeta)$ . For calculating the value of

$\phi_0 e^{\frac{1}{2}\zeta}$  in this region we use the energy dependence of the saturation scale  $Q_s^2(Y) \propto \exp(\lambda Y)$  from Ref. [87] ( $\lambda = 0.204$ ) and value of  $\phi_0 \approx 0.3$ . Note that the ratio decreases at large values of  $\phi_0 e^{\frac{1}{2}\zeta}$ , but gives a sufficiently large value  $R \approx 0.5 - 0.75$  in the LHC kinematic region.

#### 4.5 Estimates for proton–nucleus scattering

In this section we would like to make estimates of the damping factor  $R$  for proton–nucleus scattering using the same approach as in the Schwimmer model (Sect. 3.4 and Fig. 11). For these estimates we replace  $\phi_0 \exp(-\frac{1}{2}\zeta)$  by  $\phi_0 S_A(b) \exp(\frac{1}{2}\zeta)$ , and assumed that  $\phi_0 S_A(b=0) = 1/3$ . For every value of  $\zeta$ ,  $b$  could be so large that the scattering amplitude becomes small and the exchange of two BFKL Pomerons, give the only contribution. We found the solution of the equation  $\phi_0 S_A(b=0) = \phi_0 S_A(b_{\text{max}}(\zeta)) \exp(\frac{1}{2}\zeta)$  and replace the numerator of Eq. (64) by the following integral:

$$\begin{aligned} &\int_{b_{\text{max}}(\zeta)}^{b_{\text{max}}(\zeta)} d^2b \left\{ \phi_\zeta'^2 \left( \phi_0 S_A(b) e^{\frac{1}{2}\zeta} \right) \right. \\ &\quad \left. + \phi_\zeta'^3 \left( \phi_0 S_A(b) e^{\frac{1}{2}\zeta} \right) \right\} e^{-\phi(2\phi_0 S_A(b) e^{\frac{1}{2}\zeta})} \\ &\quad + \int_{b_{\text{max}}(\zeta)} d^2b \left( \phi_0 S_A(b) e^{\frac{1}{2}\zeta} \right)^2 \end{aligned} \quad (65)$$

The dominator has the form:

$$\begin{aligned} &\int_{b_{\text{max}}(\zeta)}^{b_{\text{max}}(\zeta)} d^2b \left( \phi_0 S_A(b) e^{\frac{1}{2}(\zeta - \frac{1}{2}\zeta)} \right)^2 \left( 1 - e^{-2\phi(\phi_0 S_A(b) e^{\frac{1}{4}\zeta})} \right)^2 \\ &\quad + \int_{b_{\text{max}}(\zeta)} d^2b \left( \phi_0 S_A(b) e^{\frac{1}{2}\zeta} \right)^2 \end{aligned} \quad (66)$$

Using Eqs. (65) and (66) we evaluate the damping factor for an experiment with the multiplicity  $n \geq 2\bar{n}$ , which is

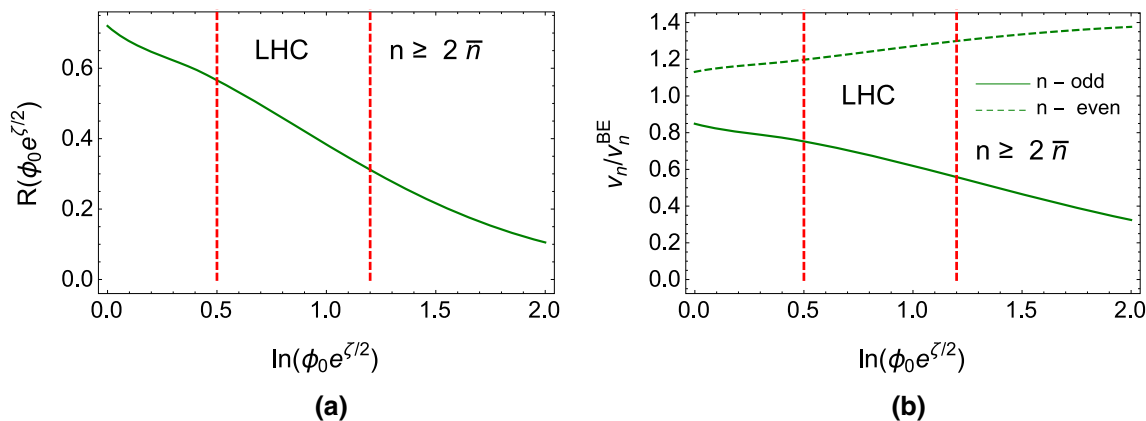


**Fig. 15** For  $n \geq 2\bar{n}$  ratio  $R$  (a) and the ratio  $v_n/v_n^{BE}$  (b and Eq. (39)) versus  $\ln(\phi_0 e^{\frac{1}{2}\zeta})$ . The vertical dotted lines show the LHC kinematic region

shown in Fig. 15a. In Fig. 15b we plot the ratio of  $v_n/v_n^{BE}$  (see Eq. (39)). This figure shows that for energies less or about the LHC energy, an experiment with the selection of the multiplicities  $n \geq 2\bar{n}$ , does not give an essential suppression for the odd harmonics.

#### 4.6 Processes with different multiplicities of produced gluons for $\tau_m \geq 1$

We now discuss DIS with nuclei, for the case where  $\tau_m = r^2 Q_s^2(A; Y = Y_{\min}) \geq 1$ , which is shown in Fig. 12b.

The general MV formula of Eq. (59) can be translated into the boundary conditions for  $\phi$  on the line  $Y = Y_{\min}$  ( $\xi_s = 0$ , see Fig. 12b and Eq. (50)) that has the following form:

$$\phi(\xi_s = 0; \xi) = \phi_0 e^\xi \tag{67}$$

For further discussion, we introduce the saturation scale at  $Y_{\min}$  in a such way that  $\xi = \ln(r^2 Q_s^2(A; Y_{\min}; b))$  and Eq. (67) give the initial condition at  $\phi_0 = 1$ .

One of the general features of solution of Eq. (60), is the increase of  $\phi$  in the saturation region (see Fig. 13). Consequently, only in the vicinity of the critical line do we need to keep term  $\exp(-\phi)$  in Eq. (55). Actually, for  $\phi_0 = 1$ , this term is not very large even at  $\zeta = 0$ , since, in our estimate we are dealing with  $\gamma + \bar{\gamma} = 2\phi_0 \approx 2$ .

Inside the saturation region we can neglect this term reducing the equation to the simple one, namely,

$$\phi_{\xi_s, \xi} = \frac{1}{4}; \quad \text{or} \quad \frac{\partial^2 \phi}{\partial t^2} - \frac{\partial^2 \phi}{\partial x^2} = \frac{1}{4} \tag{68}$$

with the initial and boundary conditions of Eqs. (57) and (67), respectively.

It is well known that the solution of this equation is different for  $t = \zeta < x$  ( $\xi < 0$ ) and  $t = \zeta > x$  ( $\xi > 0$ ) [83]. For  $t = \zeta < x$  ( $\xi < 0$ ) the solution is not affected by the

boundary conditions, and it has the form

$$\phi_1(z) = \frac{1}{8}\zeta^2 + \frac{1}{2}(e^{\phi_0} - 1)\zeta + \phi_0 \tag{69}$$

Note, that for  $\phi_0$  not small, the initial condition of Eq. (50) reads as follows

$$\phi(\zeta = 0) = \phi_0; \quad \frac{d\phi(\zeta)}{d\zeta} = \frac{1}{2}(e^{\phi_0} - 1); \tag{70}$$

The general solution to Eq. (68) has the form:

$$\phi(\xi_s, \xi) = \frac{1}{4}\xi_s \xi + F_1(\xi_s) + F_2(\xi) \tag{71}$$

Using the restriction from Eq. (57), the solution of Eq. (68) can be obtained from Eq. (71). For  $t = \zeta > x$  ( $\xi > 0$ ) we need to take into account the boundary condition of Eq. (67). Using the general solution in the form of Eq. (71), and the matching condition on the line  $\xi = 0$

$$\phi_1(\xi = 0) = \phi_2(\xi = 0) \tag{72}$$

simultaneously with the boundary conditions that have the form

$$\phi_2(\xi_s = 0) = \phi_0 e^\xi \tag{73}$$

we obtain the following solution for  $\xi > 0$

$$\phi_2(z, \xi) = \zeta^2/8 - \xi^2/8 + \phi_0 e^\xi + \frac{1}{2}(e^{\phi_0} - 1)\xi_s \tag{74}$$

Therefore, the solution to the simplified Eq. (68) has the following form

$$\phi(\zeta, \xi) = \begin{cases} \phi_1(\zeta) & \text{for } \xi \leq 0; \\ \phi_2(\zeta, \xi) & \text{for } \xi > 0; \end{cases} \tag{75}$$

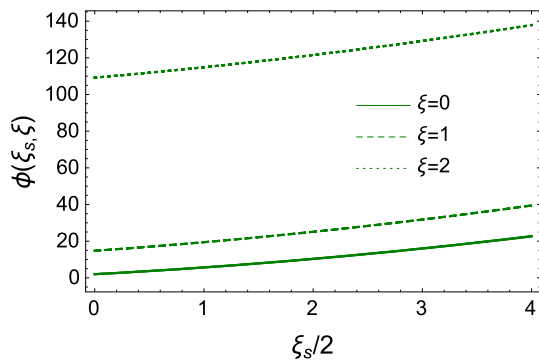


**Fig. 16** Comparison of the solutions of Eq. (76) and of Eq. (74) with the exact numerical solutions which satisfies the initial and boundary conditions of Eqs. (72) and (73). The solutions with the same  $\xi$  are marked by the same type of lines. One can see that they all coincide for  $\frac{1}{2}\xi_s \leq 4$ . The value of  $\phi_0$  was taken to be 2 as follows from Eq. (78)

For the solution of the general Eq. (55) we have

$$\phi(\xi_s, \xi) = \begin{cases} \phi(\zeta; \text{Eq. (60)}) & \text{for } \xi \leq 0; \\ \phi(\xi_s + \xi; \text{Eq. (60)}) - \phi(\xi; \text{Eq. (60)}) \\ + \phi_0 e^{\xi} & \text{for } \xi > 0; \end{cases} \quad (76)$$

where  $\phi(\zeta; \text{Eq. (60)})$  is the solution to Eq. (60) with the initial condition of Eq. (70).

The solution of Eq. (76) satisfies the initial and boundary conditions of Eqs. (72) and (73), but for  $\xi > 0$  this solution leads to the equation

$$\frac{\partial^2 \phi(\xi_s, \xi)}{\partial \xi_s \partial \xi} = \frac{1}{4} \left( 1 - e^{-\phi(\xi_s + \xi; \text{Eq. (60)})} \right) \neq \frac{1}{4} \left( 1 - e^{-\phi(\xi_s, \xi)} \right) \quad (77)$$

We found that this simple solution approaches the solution for the equation which we found numerically solving Eq. (55), with the initial and boundary conditions of Eqs. (72) and (73). In Fig. 16 we compare the solutions of Eq. (76), Eq. (74) and the numerical solution for different values of  $\xi$ . The difference for  $\xi \leq 8$  is not large, and Eq. (76) can be used for obtaining estimates. It should be noted that the simple solution of Eq. (74) provides a good approximation of the numerical solution for  $\gamma \sim \phi_0 \approx 2$ , which we need to estimate the damping factor.

The solution of Eq. (76) does not show geometric scaling behavior, and the solution of Eq. (55) depends both on  $\zeta = \xi_s + \xi$  and  $\xi$ .

We need to generalize Eq. (61) replacing  $\phi$  in this formula by Eq. (76) which results in the following expression

$$\begin{aligned} & \phi(\gamma + \bar{\gamma} - \gamma_{\text{in}}, \xi_s, \xi) \\ &= \phi \left( \ln(\gamma + \bar{\gamma} - \gamma_{\text{in}}) + \frac{1}{2}\xi_s + \frac{1}{2}\xi; \text{Eq. (60)} \right) \\ & - \phi \left( \ln(\gamma + \bar{\gamma} - \gamma_{\text{in}}) + \frac{1}{2}\xi_s; \text{Eq. (60)} \right) + \phi_0 e^{\xi} \quad (78) \end{aligned}$$

Using Eq. (78) we can calculate

$$\begin{aligned} \sigma_0^{\text{CD}} + \sigma_1^{\text{CD}} &= \frac{1}{4} \Gamma^2 (2P \rightarrow 2G) \left\{ \gamma \bar{\gamma} \phi_{\gamma'}'^2(\gamma + \bar{\gamma}, \xi_s, \xi) \right. \\ & \left. + \gamma \bar{\gamma} \gamma_{\text{in}} \phi_{\gamma'}'^3(\gamma + \bar{\gamma}, \xi_s, \xi) \right\} e^{-\phi(\gamma + \bar{\gamma}, \xi_s, \xi)} \quad (79) \end{aligned}$$

In Fig. 16 we show that the solution of Eq. (76) depends on the value of  $\xi$ . Hence, we can expect that the value of the damping factor  $R$  will depend on  $\xi$ . In Fig. 17 we plot this dependence for  $y_1 \approx y_2$  summing over all values of  $y_1$ . The damping factor  $R$  decreases, and becomes negligible at  $\xi \sim 0.4$ . Therefore, we see the full restoration of azimuthal angular symmetry  $\phi \rightarrow \pi - \phi$ , at  $\xi \geq 0.4$ .

In Sect. III-D we used the small experimental value of the triple Pomeron vertex, to show that the typical size of the nucleon is so small, that we can safely use the geometric scaling behaviour to estimate the value of the damping factor. We also know that the triple Pomeron experimental vertex, does not show any sizable dependence on the momentum transferred of interacting Pomerons. This can be interpreted as the small typical radius of the proton-nucleus interaction. In all attempts to describe the interaction of protons at high energy, the small size of the proton components appears in different ways (see Refs. [84–86] for example where  $r_{\text{proton}} \sim 0.2 \text{ GeV}^{-1}$ ). For such small sizes we face the situation shown in Fig. 12a, for which we have a large violation of  $\phi \rightarrow \pi - \phi$  symmetry.

However, for a very dense system, where the number of sources are large, the value of  $Q_s^2(A; Y_{\text{min}}; b) \propto Q_s^2(Y_{\text{min}}) S_A(b) \propto Q_s^2(Y_{\text{min}}) A^{1/3}$ , we always have the situation shown in Fig. 12b and we deal with the violation of the geometric scaling behaviour for  $\xi > 0$  which results in the restoration of the  $\phi \rightarrow \pi - \phi$  azimuthal angular symmetry, even for the events with multiplicities  $n \geq 2\bar{n}$ . For realistic heavy nuclei (gold, lead etc.),  $S_A(b=0) \sim 2$ , and we could expect a large violation of this symmetry, due to the selection of events with respect to their multiplicities. However, the estimates for  $y_1 \approx y_2 = \frac{1}{2}Y$ , shows that such expectations are premature (see Fig. 17). Nevertheless, it is ought to be noted that in a real experiment we measure the produced gluons with rather large values of the transverse momenta which leads to  $\xi < 0$ , and we have to deal with the damping factor in Fig. 12b, but in the region where we have geometric scaling behaviour of the scattering amplitude. In this region the value of the ratio  $R$ , can be obtained from Fig. 17b at

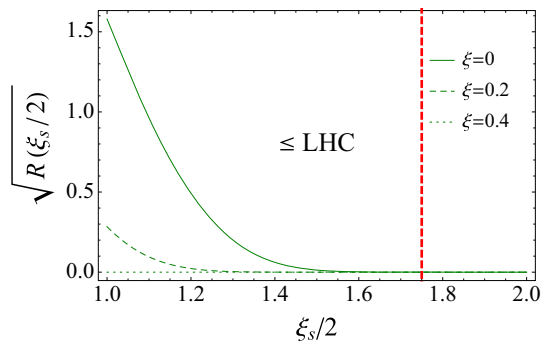


**Fig. 17** The damping factor  $\sqrt{R}$  at different values of  $\xi_s$ . For estimates for  $\xi_s$  in the LHC kinematic region, we use  $Q_s^2 \propto (1/x)^\lambda$  with  $\lambda \approx 0.2$  [87]. The damping factor is plotted for  $y_1 \approx y_2 = \frac{1}{2}Y$

$\xi = 0$ . One can see that in this case we have a rather strong violation of  $\phi \rightarrow \pi - \phi$  azimuthal angular symmetry.

## 5 Conclusions

In this paper we demonstrated that the selection of the events with different multiplicities of produced particles lead to the violation of  $\phi \rightarrow \pi - \phi$  symmetry. We found that for DIS, if  $Q^2$  is so large that  $Q^2 > Q_s^2(A; Y_{\min}; b)$  the violation of  $\phi \rightarrow \pi - \phi$  symmetry turns out to be so large, that we can neglect in the first approximation the existence of this symmetry. For such  $Q^2$  our estimates show that in the case, when the events with multiplicities  $n \geq 2\bar{n}$  are selected, we do not expect any suppression of  $v_n$  for odd  $n$  for the LHC energies or lower.  $\bar{n}$  is the mean multiplicity at a given energy. However, for  $Q^2 < Q_s^2(A; Y_{\min}; b)$  we found that for  $\xi > 0.4$ , we can neglect the violation of the symmetry and, therefore, we expect that  $v_n$  with odd  $n$ , are small.

Bearing this in mind, we claim that the character of proton-nucleus scattering depends crucially on the size of the typical dipole inside the nucleon. There are several phenomenological observations that support a rather small typical radius in the nucleon, which we have discussed in the previous section.

We hope that this paper will stimulate the discussion of the angular correlations in the events with fixed multiplicities of produced particles, which crucially influence these correlations.

**Acknowledgements** We thank our colleagues at Tel Aviv university and UTFSM for encouraging discussions. This research was supported by the BSF Grant 2012124, by Proyecto Basal FB 0821 (Chile), Fondecyt (Chile) Grant 1180118 and by CONICYT Grant PIA ACT1406.

**Open Access** This article is distributed under the terms of the Creative Commons Attribution 4.0 International License (<http://creativecommons.org/licenses/by/4.0/>), which permits unrestricted use, distribution, and reproduction in any medium, provided you give appropriate credit to the original author(s) and the source, provide a link to the Creative Commons license, and indicate if changes were made. Funded by SCOAP<sup>3</sup>.

## References

1. J. Adams, [STAR Collaboration], Phys. Rev. Lett. **95**, 152301 (2005). [arXiv:nucl-ex/0501016](#)
2. A. Adare et al., [PHENIX Collaboration], Phys. Rev. C **78**, 014901 (2008). [arXiv:0801.4545](#) [nucl-ex]
3. B. Alver et al., [PHOBOS Collaboration], Phys. Rev. Lett. **104**, 062301 (2010). [arXiv:0903.2811](#) [nucl-ex]
4. B.I. Abelev et al., [STAR Collaboration], Phys. Rev. C **80**, 064912 (2009). [arXiv:0909.0191](#) [nucl-ex]
5. V. Khachatryan et al., [CMS Collaboration], JHEP **1009**, 091 (2010). [arXiv:1009.4122](#) [hep-ex]
6. S. Chatrchyan et al., [CMS Collaboration], Phys. Lett. B **718**, 795 (2013). [arXiv:1210.5482](#) [nucl-ex]
7. S. Chatrchyan et al., [CMS Collaboration], Phys. Lett. B **724**, 213 (2013). [arXiv:1305.0609](#) [nucl-ex]
8. S. Chatrchyan et al., [CMS Collaboration], JHEP **1402**, 088 (2014). [arXiv:1312.1845](#) [nucl-ex]
9. S. Chatrchyan et al., [CMS Collaboration], Phys. Rev. C **89**(4), 044906 (2014). [arXiv:1310.8651](#) [nucl-ex]
10. B. Abelev et al., [ALICE Collaboration], Phys. Lett. B **719**, 29 (2013). [arXiv:1212.2001](#) [nucl-ex]
11. B. B. Abelev et al., [ALICE Collaboration], Phys. Rev. C **90**(5), 054901 (2014). [arXiv:1406.2474](#) [nucl-ex]
12. Y. Zhou, [ALICE Collaboration], J. Phys. Conf. Ser. **509**, 012029 (2014)
13. B. Abelev et al., [ALICE Collaboration], Phys. Lett. B **719**, 29 (2013). [arXiv:1212.2001](#) [nucl-ex]
14. G. Aad et al., [ATLAS Collaboration], Phys. Rev. C **90**(4), 044906 (2014). [arXiv:1409.1792](#) [hep-ex]
15. B. Wosiek, [ATLAS Collaboration], Ann. Phys. **352**, 117 (2015)
16. G. Aad et al., [ATLAS Collaboration], Phys. Lett. B **725**, 60 (2013). [arXiv:1303.2084](#) [hep-ex]
17. G. Aad et al., [ATLAS Collaboration], Phys. Rev. Lett. **116**, 172301 (2016). [arXiv:1509.04776](#) [hep-ex]
18. E. Gotsman, E. Levin, I. Potashnikova, Eur. Phys. J. C **77**(9), 632 (2017). [arXiv:1706.07617](#) [hep-ph]
19. E. Gotsman, E. Levin, Phys. Rev. D **96**, 074011 (2017). [arXiv:1705.07406](#) [hep-ph]
20. E. Gotsman, E. Levin, U. Maor, Eur. Phys. J. C **76**(11), 607 (2016). [arXiv:1607.00594](#) [hep-ph]
21. Y.V. Kovchegov, E. Levin, *Quantum Chromodynamics at High Energy*, vol. 33 (Cambridge University Press, Cambridge, 2012)
22. A. Kovner, M. Lublinsky, Phys. Rev. D **83**, 034017 (2011). [arXiv:1012.3398](#) [hep-ph]
23. Y.V. Kovchegov, D.E. Wertepny, Nucl. Phys. A **906**, 50 (2013). [arXiv:1212.1195](#) [hep-ph]
24. T. Altinoluk, N. Armesto, G. Beuf, A. Kovner, M. Lublinsky, Phys. Lett. B **752**, 113 (2016). [arXiv:1509.03223](#) [hep-ph]
25. T. Altinoluk, N. Armesto, G. Beuf, A. Kovner, M. Lublinsky, Phys. Lett. B **751**, 448 (2015). [arXiv:1503.07126](#) [hep-ph]
26. E. Gotsman, E. Levin, Phys. Rev. D **95**(1), 014034 (2017). [arXiv:1611.01653](#) [hep-ph]
27. A. Kovner, M. Lublinsky, V. Skokov, Exploring correlations in the CGC wave function: odd azimuthal anisotropy. [arXiv:1612.07790](#) [hep-ph]
28. K. Dusling, R. Venugopalan, Phys. Rev. D **87**(9), 094034 (2013). [arXiv:1302.7018](#) [hep-ph] (and reference therein)
29. A. Kovner, M. Lublinsky, Int. J. Mod. Phys. E **22**, 1330001 (2013). [arXiv:1211.1928](#) [hep-ph] (and references therein)
30. Y.V. Kovchegov, V.V. Skokov, When gluons go odd: how classical gluon fields generate odd azimuthal harmonics for the two-gluon correlation function in high-energy collisions. [arXiv:1802.08166](#) [hep-ph]
31. A.H. Mueller, Phys. Rev. D **2**, 2963 (1970)

32. V.S. Fadin, E.A. Kuraev, L.N. Lipatov, Phys. Lett. B **60**, 50 (1975)
33. E.A. Kuraev, L.N. Lipatov, V.S. Fadin, Sov. Phys. JETP **45**, 199 (1977) (Zh Eksp Teor Fiz 72, 377, 1977)
34. I.I. Balitsky, L.N. Lipatov, Sov. J. Nucl. Phys. **28**, 822 (1978) (Yad Fiz 28, 1597, 1978)
35. M.A. Braun, Phys. Lett. B **632**, 297 (2006). [arXiv:hep-ph/0512057](#)
36. M.A. Braun, Eur. Phys. J. C **16**, 337 (2000). [arXiv:hep-ph/0001268](#)
37. M.A. Braun, Phys. Lett. B **483**, 115 (2000). [arXiv:hep-ph/0003004](#)
38. M.A. Braun, Eur. Phys. J. C **33**, 113 (2004). [arXiv:hep-ph/0309293](#)
39. M.A. Braun, Eur. Phys. J. C **6**, 321 (1999). [arXiv:hep-ph/9706373](#)
40. M.A. Braun, G.P. Vacca, Eur. Phys. J. C **6**, 147 (1999). [arXiv:hep-ph/9711486](#)
41. E. Levin, M. Lublinsky, Nucl. Phys. A **763**, 172 (2005). [arXiv:hep-ph/0501173](#)
42. E. Levin, J. Miller, A. Prygarin, Nucl. Phys. A **806**, 245 (2008). [arXiv:0706.2944](#) [hep-ph]
43. T. Altinoluk, C. Contreras, A. Kovner, E. Levin, M. Lublinsky, A. Shulkin, JHEP **1309**, 115 (2013). [arXiv:1306.2794](#) [hep-ph]
44. T. Altinoluk, A. Kovner, E. Levin, M. Lublinsky, JHEP **1404**, 075 (2014). [https://doi.org/10.1007/JHEP04\(2014\)075](https://doi.org/10.1007/JHEP04(2014)075). [arXiv:1401.7431](#) [hep-ph]
45. V.A. Abramovsky, V.N. Gribov, O.V. Kancheli, Yad. Fiz. **18**, 595 (1973)
46. V.A. Abramovsky, V.N. Gribov, O.V. Kancheli, Sov. J. Nucl. Phys **18**, 308 (1974)
47. Y.V. Kovchegov, Phys. Rev. D **64**, 114016 (2001) (erratum-ibid. D 68, 039901, 2003). [arXiv:hep-ph/0107256](#)
48. Y.V. Kovchegov, K. Tuchin, Phys. Rev. D **65**, 074026 (2002). [arXiv:hep-ph/0111362](#)
49. J. Jalilian-Marian, Y.V. Kovchegov, Phys. Rev. D **70**, 114017 (2004) (erratum-ibid. D 71, 079901, 2005). [arXiv:hep-ph/0405266](#)
50. M.A. Braun, Eur. Phys. J. C **48**, 501 (2006). [arXiv:hep-ph/0603060](#)
51. C. Marquet, Nucl. Phys. B **705**, 319 (2005). [arXiv:hep-ph/0409023](#)
52. A. Kovner, M. Lublinsky, JHEP **0611**, 083 (2006). [arXiv:hep-ph/0609227](#)
53. E. Levin, A. Prygarin, Phys. Rev. C **78**, 065202 (2008). [arXiv:0804.4747](#) [hep-ph]
54. J. Jalilian-Marian, Y.V. Kovchegov, Phys. Rev. D **70**, 114017 (2004) (erratum-ibid. D 71, 079901, 2005). [arXiv:hep-ph/0405266](#)
55. I. Balitsky, [arXiv:hep-ph/9509348](#)
56. I. Balitsky, Phys. Rev. D **60**, 014020 (1999). [arXiv:hep-ph/9812311](#)
57. Y.V. Kovchegov, Phys. Rev. D **60**, 034008 (1999). [arXiv:hep-ph/9901281](#)
58. A.H. Mueller, Nucl. Phys. B **415**, 373 (1994)
59. A.H. Mueller, Nucl. Phys. B **437**, 107 (1995)
60. E. Levin, M. Lublinsky, Nucl. Phys. A **730**, 191 (2004). [arXiv:hep-ph/0308279](#)
61. E. Levin, M. Lublinsky, Phys. Lett. B **607**, 131 (2005). [arXiv:hep-ph/0411121](#)
62. Y.V. Kovchegov, E. Levin, Nucl. Phys. B **577**, 221 (2000). [arXiv:hep-ph/9911523](#)
63. S. Bondarenko, E. Gotsman, E. Levin, U. Maor, Nucl. Phys. A **683**, 649 (2001). [arXiv:hep-ph/0001260](#)
64. K.G. Boreskov, A.B. Kaidalov, V.A. Khoze, A.D. Martin, M.G. Ryskin, Eur. Phys. J. C **44**, 523 (2005). [arXiv:hep-ph/0506211](#)
65. E. Levin, A. Prygarin, Eur. Phys. J. C **53**, 385 (2008). [arXiv:hep-ph/0701178](#)
66. I.A. Verdiev, O.V. Kancheli, S.G. Matinyan, A.M. Popova, K.A. Ter-Martirosyan, Sov. Phys. JETP **19**, 1148 (1964)
67. J. Finkelstein, K. Kajantie, Phys. Lett. **26B**, 305 (1968)
68. H.D.I. Abarbanel, J.B. Bronzan, R.L. Sugar, A.R. White, Phys. Rep. **21**, 119 (1975)
69. V.A. Khoze, A.D. Martin, M.G. Ryskin, Phys. Lett. B **780**, 352 (2018). [arXiv:1801.07065](#) [hep-ph]
70. V.A. Khoze, A.D. Martin, M.G. Ryskin, Phys. Lett. B **437**, 408 (1998) (and references therein)
71. A. Schwimmer, Nucl. Phys. B **94**, 445 (1975)
72. E. Gotsman, E. Levin, U. Maor, Eur. Phys. J. C **75**(5), (2015), 179. <https://doi.org/10.1140/epjc/s10052-015-3399-4>. [arXiv:1502.05202](#) [hep-ph]
73. A. Kormilitzin, E. Levin, A. Prygarin, Nucl. Phys. A **813**, 1 (2008). [arXiv:0807.3413](#) [hep-ph]
74. E. Levin, K. Tuchin, Nucl. Phys. B **573**, 833 (2000). [arXiv:hep-ph/9908317](#)
75. E. Levin, JHEP **1311**, 039 (2013). [arXiv:1308.5052](#) [hep-ph]
76. A. Kormilitzin, E. Levin, S. Tapia, Nucl. Phys. A **872**, 245 (2011). [arXiv:1106.3268](#) [hep-ph]
77. V.N. Gribov, L.N. Lipatov, Sov. J. Nucl. Phys **15**, 438 (1972)
78. G. Altarelli, G. Parisi, Nucl. Phys. B **126**, 298 (1977)
79. Yu I Dokshitser, Sov. Phys. JETP **46**, 641 (1977)
80. E. Iancu, K. Itakura, L. McLerran, Nucl. Phys. A **708**, 327 (2002). [arXiv:hep-ph/0203137](#)
81. A.H. Mueller, D.N. Triantafyllopoulos, Nucl. Phys. B **640**, 331 (2002). [arXiv:hep-ph/0205167](#)
82. D.N. Triantafyllopoulos, Nucl. Phys. B **648**, 293 (2003). [arXiv:hep-ph/0209121](#)
83. Andrei D. Polyaniin, Valentin F. Zaitsev, *Handbook of Nonlinear Partial Differential Equations* (Chapman & Hall/CRC, London, 2004)
84. E. Gotsman, E. Levin, I. Potashnikova, Phys. Lett. B **781**, 155 (2018). [arXiv:1712.06992](#) [hep-ph]
85. E. Gotsman, E. Levin, I. Potashnikova, Eur. Phys. J. C **77**(9), 632 (2017). [arXiv:1706.07617](#) [hep-ph]
86. E. Gotsman, E. Levin, U. Maor, Eur. Phys. J. C **75**(5), 179 (2015). [arXiv:1502.05202](#) [hep-ph]
87. A. Dumitru, D.E. Kharzeev, E.M. Levin, Y. Nara, Phys. Rev. C **85**, 044920 (2012). [arXiv:1111.3031](#) [hep-ph]
88. L. McLerran, R. Venugopalan, Phys. Rev. D **49**(2233), 3352 (1994)
89. L. McLerran, R. Venugopalan, Phys. Rev. D **50**, 2225 (1994)
90. L. McLerran, R. Venugopalan, Phys. Rev. D **53**, 458 (1996)
91. L. McLerran, R. Venugopalan, Phys. Rev. D **59**, 09400 (1999)